TECHNICAL REPORT N-72-7

FUNDAMENTAL STUDIES OF MEDIUM-STRUCTURE INTERACTION

Report 1

FINITE ELEMENT ANALYSIS OF BURIED CYLINDERS

by

J. L. Kirkland, R. E. Walker

June 1972

Sponsored by Defense Nuclear Agency

Conducted by U. S. Army Engineer Waterways Experiment Station
Weapons Effects Laboratory
Vicksburg, Mississippi

TECHNICAL REPORT N-72-7

FUNDAMENTAL STUDIES OF MEDIUM-STRUCTURE INTERACTION

Report 1

FINITE ELEMENT ANALYSIS OF BURIED CYLINDERS

by

J. L. Kirkland, R. E. Walker

June 1972

Sponsored by Defense Nuclear Agency

Conducted by U. S. Army Engineer Waterways Experiment Station
Weapons Effects Laboratory
Vicksburg, Mississippi

ARMY-MRC VICKSBURG, MISS.

ABSTRACT

A finite element computer program developed by the University of California, Berkeley, was adopted and modified to perform static analysis of buried structures. Two separate variable-moduli soil models were used in the code to analyze the response of 6-inch-diameter cylinders having wall thicknesses of 1/8, 1/4, and 3/8 inch when buried to a depth of 9 inches in dry sand and subjected to a static overpressure. The computed results were compared with experimental results obtained from static tests of these cylinders in the Waterways Experiment Station Small Blast Load Generator.

The computer code developed generally yielded a fair approximation of the structural response of the cylinders tested with either of the two soil models employed. The major area of discrepancy between experimental and calculated results was in the values of moment and thrust for the thicker cylinders. The nature of these discrepancies indicates that the expected lateral support of the cylinders did not develop in the experiments. This fact is explained by the possible existence of an area of low-density soil below the spring line and adjacent to the cylinder (the region where sand placement is most difficult).

The code, in general, represents a reasonable method for predicting the response of buried cylinders, and undoubtedly other geometries as well. However, analysis of stiff cylinders is confounded by the fact that a detailed knowledge of the interface zone is needed because of the small motion of the spring line of such stiff cylinders.

PREFACE

This report was prepared in the Weapons Effects Laboratory of the U. S. Army Engineer Waterways Experiment Station (WES), under the sponsorship of the Defense Nuclear Agency (formerly Defense Atomic Support Agency). The work was accomplished during the period from March through December 1970. During this time, Mr. G. L. Arbuthnot, Jr., was chief of the Weapons Effects Laboratory. This report was prepared by Dr. J. L. Kirkland and Mr. R. E. Walker under the supervision of Mr. W. J. Flathau, Chief, Protective Structures Branch.

The computer code used in this analysis was based on a code partially developed by the University of California, Berkeley, under contract DACA 39-67-C-0020, DASA-SC210. The experimental data were obtained as part of an experimental investigation, also supported by the Defense Nuclear Agency, conducted by Dr. J. D. Prendergast, formerly of WES. Grateful appreciation is extended to him for making the data available and for his helpful comments concerning the experimental procedure.

Directors of the WES during the preparation and publication of this report were COL Levi A. Brown, CE, and COL Ernest D. Peixotto, CE. Technical Director was Mr. F. R. Brown.

CONTENTS

NOTATION

$A_1, A_2, \ldots$	Localized Ritz parameters
$[B]$	Strain-nodal point displacement matrix
$[D]$	Constitutive matrix
e	Volumetric strain
$\underset{\sim}{E}$	Unit matrix
$\{F\}$	Nodal point loads
$\{F^i\}$	Nodal point forces of element i
G	Shear modulus
G_o , G_{oU}	Curve-fitting constants
$[H]$	Stress-nodal point displacement matrix
I_1, I_2, I_3	Invariants of strain tensor
I_2'	Second invariant of the deviator strain
K	Bulk modulus
$[K]$	Stiffness matrix for the complete structure
$[K^i]$	Stiffness matrix for element i
M	Constrained modulus
$[M]$	Displacement transformation matrix
$[N]$	Strain transformation matrix
P	Mean stress
P_c	Critical pressure defining the change in slope of the failure envelope
S_2	Second invariant of the deviator stress
$\underset{\sim}{S}$	Deviatoric stress tensor
$\underset{\sim}{S}_2$	Deviatoric stress tensor associated with ϕ_2
u	Displacement in x direction
$\{u\}$	Nodal point displacement vectors
$\{u^i\}, \{v^i\}$	Nodal point displacements of element i
v	Displacement in y direction
W_E	External virtual work
W_I	Internal virtual work
α	Drucker-Prager constant

γ_1, γ_2, etc.	Curve-fitting constants
δ_{ij}	Elements of unit matrix
$\{\Delta\varepsilon\}$	Incremental strain vectors
$\{\Delta\sigma\}$	Incremental stress vectors
ε'_{ij}	Elements of deviatoric strain tensor
ε_x	Strain in x direction
ε_{xy}	Shear strain
ε_y	Strain in y direction
ε_z	Strain in z direction
$\underset{\sim}{\varepsilon}$	Strain tensor
$\underset{\sim}{\varepsilon}'$	Deviatoric strain tensor
$\{\varepsilon\}$	Strain vectors
μ	Shear modulus (initial tangent)
σ'_{ij}	Elements of deviatoric stress tensor
σ_r	Stress in r radial direction
σ_x	Stress in x direction
σ_{xy}	Shear stress
σ_y	Stress in y direction
σ_z	Stress in z axial direction
$\underset{\sim}{\sigma}$	Stress tensor
$\underset{\sim}{\sigma}_2$	Stress tensor associated with ϕ_2
$\{\sigma\}$	Stress vectors
$\overline{\sigma}$	Maximal value of the second invariant of the deviator stress
ϕ	Total inner energy
ϕ_2	Inner energy associated with shear

CONVERSION FACTORS, BRITISH TO METRIC UNITS OF MEASUREMENT

British units of measurement used in this report can be converted to metric units as follows:

Multiply	By	To Obtain
feet	0.3048	meters
inches	25.4	millimeters
inch-pounds	0.1129848	meter-newtons
pounds (force)	4.448222	newtons
pounds (force) per square inch	6.894757	kilonewtons per square meter

CHAPTER 1

INTRODUCTION

1.1 BACKGROUND

The need to design buried cylinders has been increased with the placing of sensitive defense and command centers underground for protection. A prime concern in underground protective construction involves the design of buried circular conduits capable of resisting the high overpressures generated by large-yield nuclear weapons (Reference 1). Such cylinders are used to encase and protect communication cables that lead to various important installations throughout the United States.

However, buried conduits have a great variety of applications and are not limited to protective construction as such. For instance, studies have been made to see if utility tunnels can be constructed to serve as shelters in case of a national emergency, and thus serve in a dual capacity (Reference 2). Also, there is a need to analyze existing utility tunnels to determine the blast resistance of such facilities. Furthermore, the cost of constructing buried conduits has been high, and methods and designs are constantly being sought to reduce this expense.

Stress analysis of buried cylinders using plane strain geometry is amenable to classical analysis (i.e., using complex variables, integral transforms, etc.) under very restrictive assumptions on the mathematical model. There is considerable literature in this area, the most exhaustive treatment being Savin's work using complex variables (Reference 3). Whereas closed-form solutions are available only for a limited class of problems, numerical solutions (not simply numerical integral evaluations), with the aid of digital computers, have been achieved under less restrictive assumptions. Two numerical methods for stress analysis have received extensive treatment in the technical literature in recent years. The first of these is the finite difference method, which is applicable if the variation in the geometry and material properties can be expressed analytically. If dynamic problems are included, there are many versions

of finite difference schemes (e.g., the Afton Codes, as described in Reference 4, and the Tensor Code); however, they will not be considered here.

The second numerical procedure is the finite element method, which is a Ritz technique of seeking a stationary value of an energy integral (References 5 and 6). This method has been employed very successfully in analyzing a wide variety of continuum mechanics problems (References 7, 8, 9, 10, and 11). In general, a variational theorem is used to produce governing field equations which are written in terms of discretized displacement variables. Static assumptions, valid over small subdomains of the body, are made, and the energy is expressed in terms of a summation of integrals over each of the subdomains. The extremization of the energy integral leads to a set of equations with the unknowns being the Ritz parameters. Thus this procedure results in a force-displacement relationship of the nodal points of the discretized domain.

1.2 PURPOSE AND SCOPE

The difficulty of predicting the response of buried structures lies with obtaining a model for the surrounding soil and its interface with the structure (Reference 12). In this study, two mathematical models using the finite element method were examined and the results compared with experimental data. Although the experimental data are for cylinders having circular cross sections, it should be mentioned that this is not required for the finite element part of the analysis.

A computer program, using FORTRAN IV language, whose basic structure was developed at the University of California, Berkeley, was adopted and modified to run the problem (see References 9 and 10). Modification of the code was time-consuming and represents a major part of this effort. However, it produced a code conveniently structured for inserting different material models with only minor changes necessary. A source deck of this code is documented and filed in the Nuclear Weapons Effects Division, U. S. Army Engineer Waterways Experiment Station (WES). The flow sequence of the computer code is explained in Chapter 4.

CHAPTER 2

FINITE ELEMENT METHOD

The majority of the direct methods of analysis used in the solution of engineering field problems are methods of approximating a minimum of the energy functional. Thus, in the Rayleigh-Ritz method, a series-type solution is used, the parameters of the series being adjusted to give a minimum to the specified functional. Similarly, the finite element method uses a series of localized functions, the magnitudes of these functions in the various regions being found from the conditions of minimum energy.

The particular shape functions used in this finite element analysis are

$$u(x,y) = A_1 + A_2x + A_3y + A_4xy$$

$$v(x,y) = A_5 + A_6x + A_7y + A_8xy \qquad (2.1)$$

Where: u = displacement in x direction

v = displacement in y direction

$A_1, A_2, \ldots$ = localized Ritz parameters

A typical quadrilateral element is shown in Figure 2.1. For plane geometry, the strain-dispacement relations are

$$\varepsilon_x = \frac{\partial u}{\partial x}$$

$$\varepsilon_y = \frac{\partial v}{\partial y}$$

$$\varepsilon_{xy} = \frac{\partial u}{\partial y} + \frac{\partial v}{\partial x} \qquad (2.2)$$

or in matrix form

$$\begin{Bmatrix} \varepsilon_x \\ \varepsilon_y \\ \varepsilon_{xy} \end{Bmatrix} = \begin{bmatrix} \frac{\partial}{\partial x} & 0 \\ 0 & \frac{\partial}{\partial y} \\ \frac{\partial}{\partial y} & \frac{\partial}{\partial x} \end{bmatrix} \begin{Bmatrix} u \\ v \end{Bmatrix}$$

which can be abbreviated as

$$\{\varepsilon\} = [N]\{u\} \tag{2.3}$$

Where: $\{\varepsilon\}$ = strain vectors

$[N]$ = strain transformation matrix

$\{u\}$ = nodal point displacement vectors

Using the condition that Equation 2.1 must hold at the node points, the role of the A's is replaced by the u^i's , resulting in

$$\{u\} = [M]\left\{u^i\right\} \tag{2.4}$$

Where: $[M]$ = displacement transformation matrix

$\left\{u^i\right\}$ = nodal point displacements of element i

which gives the displacement field within the element in terms of the nodal point displacements.

Using Equation 2.4 in Equation 2.3 gives

$$\{\varepsilon\} = [B]\left\{u^i\right\} \tag{2.5}$$

where $[B] = [N][M]$. Equation 2.5 is called the strain-displacement transformation matrix.

In a global sense, we simply monitor the movement of a discrete set of judiciously picked particles, and, once their motion is determined, the field variables within an element are known from Equation 2.4.

Letting [D] represent the constitutive matrix, the stress vectors are given by

$$\{\sigma\} = [D]\{\varepsilon\} \tag{2.6}$$

From Equations 2.5 and 2.6

$$\{\sigma\} = [H]\left\{u^i\right\} \tag{2.7}$$

Where: $[H] = [D][B]$

Applying the principle of virtual work

$$W_I = \int_V \{\varepsilon\}^T\{\sigma\}\, dv \tag{2.8}$$

where W_I is the work associated with the stresses internal to the element when the node points take on a virtual displacement $\left\{v^i\right\}$, $\{\varepsilon\}^T$ is the transpose, and the integral is over the volume of the element. Also

$$W_E = \left\{v^i\right\}^T\left\{F^i\right\} \tag{2.9}$$

where W_E is the work done by the nodal forces during the same displacement of the nodal points $\left\{v^i\right\}$, and $\left\{F^i\right\}$ are the nodal point forces of element i. Equating Equations 2.8 and 2.9

$$\left\{v^i\right\}^T\left\{F^i\right\} = \int_V \{\varepsilon\}^T\{\sigma\}\, dv \tag{2.10}$$

Using Equation 2.5 in Equation 2.10

$$\left\{v^i\right\}^T\left\{F^i\right\} = \left\{v^i\right\}^T\int_V [B]^T\{\sigma\}\, dv \tag{2.11}$$

where $\left\{v^i\right\}$ are arbitrary virtual displacements and need only be compatible with the constraints of the system.

Letting $\left\{v^i\right\}$ be unit displacements

$$\left\{F^i\right\} = \int [B]^T \{\sigma\}\, dv \tag{2.12}$$

Using Equations 2.7 and 2.12 and considering a general displacement $\left\{u^i\right\}$

$$\left\{F^i\right\} = \int [B]^T [D][B]\, dv \left\{u^i\right\} \tag{2.13}$$

or defining

$$\left[K^i\right] = \int [B]^T [D][B]\, dv$$

Equation 2.13 becomes

$$\left\{F^i\right\} = \left[K^i\right] \left\{u^i\right\} \tag{2.14}$$

Thus, $\left[K^i\right]$ relates generalized forces and deformations and is called the element stiffness matrix. Each term of this matrix defines the value of a particular force parameter associated with deformation of the element in a particular mode by a unit amount. It is important to recognize that in a plane problem, as is the case here, the nodal "points" are in reality lines of unit length in plan view of the finite element grid.

The stiffness matrix for the entire system of elements is constructed by combining all the elemental stiffness matrices. The solution proceeds by solving this system of equations represented by

$$[K]\{u\} = \{F\} \tag{2.15}$$

for the displacements $\{u\}$, where $[K]$ is the stiffness matrix for the entire system of elements and $\{F\}$ are the nodal point loads.

The complexity of the method lies in the massive amount of algebra involved in its use. However, in practical systems, the stiffness matrix $[K]$ is only sparsely populated; therefore, by properly labeling the node points, a banded matrix results, and thus special techniques can

be developed for treating the large set of equations. The secret to the wide acceptance of the finite element method lies in the ease with which it treats local variations of the field variables. On the other hand, finite difference schemes that evolve from differential equations are expressed in global coordinates, and treating local variations is, in general, difficult.

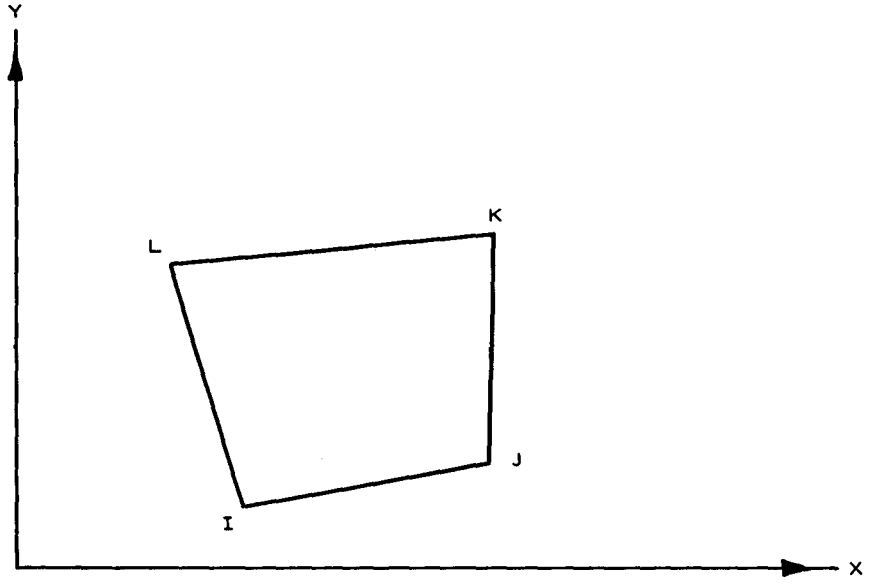

Figure 2.1 A typical element.

CHAPTER 3

SOIL MODELS

There are certain to be many questions arising in any effort to analyze problems involving soil as a continuum medium. Two salient ones are:

1. How to generalize the few loading paths (treating the stress tensor as a vector in stress space) which can be reasonably tested to any loading path which may be developed in a given element in the course of loading a finite element representation of the structure.

2. What nonlinear aspects of the soil behavior are most influential in governing the motions of the problem.

The approach to the constitutive equations of an equivalent soil continuum will be highly influenced by the fact that the problem will be solved using a computer. That is, the final solution will be the result of working a sequence of linear elastic problems and combining them so as to reflect the nonlinearities that are known to exist in the global problem. The problem faced here--that is, of constructing a nonlinear model for the soil based on very limited test information--is not new; it only appears more acute due to the recent attempts to use such highly sophisticated computer codes to solve problems which involve soil as a medium.

In applying incremental numerical techniques to problems of soil stress and deformation, it seems highly desirable to utilize the flexibility of the calculational method to the fullest by including the most realistic material behavior possible. This is particularly important since the nonlinearities of soil stress-strain behavior are easily recognized, and the manner in which it should be linearized is not clear (References 12, 13, and 14). Furthermore, the literature of soil mechanics affords little guidance in the matter of selecting either linear or nonlinear soil characteristics for use in a given problem.

The incremental numerical technique for solving nonlinear soil mechanics problems is based on the assumption that the nonlinear material response function may be replaced with a piecewise linear response

function. Thus, the effort in this case is reduced to solving a succession of similar problems. This is accomplished by partitioning the inputs into successive increments. Each input increment is assumed to be small enough so that the resulting incremental stresses and deformations are linearly related. This connection between the incremental stresses and strains remains unchanged during the increment; the values of the bulk and shear moduli depend upon the total strain invariants prior to the increment.

Therefore, the treatment followed here is one of assuming incremental isotropy in forming the stiffness matrix for each load step. Perhaps it is more reasonable to claim that a "new material" is loaded in each incremental problem and that, although this new material may be stiffer than the last material that occupied this element, it is still isotropic with respect to this load increment. Physically, this implies that the soil stiffens (or softens) in all directions by the same amount based on the current total volumetric and deviatoric strains.

Of course, the meaning of the assumption of incremental isotropy and small deformation theory is that each displacement field resulting from an increment of load is calculated from the original reference configuration. Although not pointed out by most authors, this is the usual technique used in computer codes. Here we see a subtle advantage in the finite element method: it emphasizes the physical significance of the assumptions involved in constructing the mathematical model.

It is important to note that the closer one examines the computer approach to problems of this type, the more it appears that, regardless of original intentions, all are solving a succession of linear incremental problems. It is the basic idea that these incremental problems will sum in such a fashion as to reflect the nonlinearities of the global problem. One immediate gain of this procedure is that it eliminates the task of having to obtain two constants which contain all the information in the stress-strain curves for soil.

3.1 JK MODEL

3.1.1 Theory. In formulating the nonlinear function representing

the shearing behavior of soils, many test results and the experience gained from interpreting these results must be used. The function representing the shearing characteristics of the soil can be required to meet the limiting behavior observed in the tests. This is the idea used in developing the first soil model (Reference 15), which is designated the JK model. The function defining the shearing behavior of this model is

$$S_2 = -\left(\frac{2\mu}{1 + \frac{2\mu}{\sqrt{\bar{\sigma}}}\sqrt{-I_2'}}\right)^2 I_2' \tag{3.1}$$

where S_2 and I_2' are the second invariants of the deviator stress and strain tensor, respectively, $\bar{\sigma}$ is the maximal second invariant of the deviator stress, and μ is shear modulus (initial tangent). As described in Appendix A, $\bar{\sigma}$ may be made a function of the first stress invariant and, in this way, the "yield" surface depends on the mean pressure P as defined in Equation 3.4. Figure 3.1 shows a plot of S_2 versus $-I_2'$ for $P = 0$.

Thus, although the model will not be classical plasticity as such, the intermediate elastic problems will be picked so that the desirable (in the sense that they are indicated by soil tests) features of plasticity will be reflected in the global problem. To emphasize the notions of plasticity, the strain energy is partitioned into volumetric and deviatoric parts, and the constitutive relations are expressed as

$$P = Ke \tag{3.2}$$

and

$$\sigma_{ij}' = 2G\varepsilon_{ij}' \tag{3.3}$$

Where:

$$P = \frac{\sigma_{11} + \sigma_{22} + \sigma_{33}}{3} \tag{3.4}$$

$$e = \varepsilon_{11} + \varepsilon_{22} + \varepsilon_{33} \tag{3.5}$$

and

K = bulk modulus

σ'_{ij} = elements of deviatoric stress tensor

ε'_{ij} = elements of deviatoric strain tensor

G = shear modulus

3.1.2 Applications. The soil medium in this soil-structure interaction problem was Cook's Bayou sand (a sand local to the Vicksburg area). Figure 3.2 indicates its behavior in a one-dimensional compression test. In this test (constrained modulus test) the sand was confined to essentially zero lateral strain while being loaded in the longitudinal direction. The behavior of the sand in this type environment gives an indication of its bulk modulus. Figure 3.3 shows the sand's behavior under triaxial test conditions and is an indication of its shearing behavior. These two figures constitute the stress-strain test data used to construct a constitutive model for an equivalent continuum that represents the sand in the finite element analysis of the problem.

The important situation here is that the boundary conditions of the constrained modulus test (Figure 3.2) require one to use some means to obtain the pressure-volume relationship expressed by Equation 3.1. This is accomplished by performing a code calculation on the constrained modulus test geometry using a one-element grid. For this case, the stress path of the element is simply the load path of the constrained modulus test. Therefore, the bulk modulus K is replaced with $M - \frac{4}{3} G$ (where M is the constrained modulus) for this calculation, and a pressure-volume curve for the soil is constructed as shown in Figure 3.4.

It should be noted that the effect of this calculation is the scaling of the σ_z axis in Figure 3.2, and, therefore, the general features of the constrained modulus curve are retained. This pressure-volume curve, along with the shearing behavior indicated by Equation 2.3,

is then used for any element containing this type soil in the finite element representation of the problem.

Using δ_{ij} for the elements of the unit matrix, Equations 3.2 and 3.3 may be combined and written as

$$\sigma_{ij} = Ke\delta_{ij} + 2G\varepsilon'_{ij} \tag{3.6}$$

Equating the components of Equation 3.6 and inserting the conditions of plane strain gives

$$\begin{Bmatrix} \sigma_x \\ \sigma_y \\ \sigma_{xy} \end{Bmatrix} = \begin{bmatrix} K + \frac{4}{3}G & K - \frac{2}{3}G & 0 \\ K - \frac{2}{3}G & K + \frac{4}{3}G & 0 \\ 0 & 0 & 2G \end{bmatrix} \begin{Bmatrix} \varepsilon_x \\ \varepsilon_y \\ \varepsilon_{xy} \end{Bmatrix} \tag{3.7}$$

Where:

$$\sigma_{11} \equiv \sigma_x \,, \quad \sigma_{22} \equiv \sigma_y \,, \quad \sigma_{12} \equiv \sigma_{xy}$$
$$\varepsilon_{11} \equiv \varepsilon_x \,, \quad \varepsilon_{22} \equiv \varepsilon_y \,, \quad \varepsilon_{12} \equiv \varepsilon_{xy}$$

From this, the connection between $\{\Delta\sigma\}$ and $\{\Delta\varepsilon\}$ for any soil element is simply expressed as

$$\{\Delta\sigma\} = [D]\{\Delta\varepsilon\} \tag{3.8}$$

Where:

$$[D] = \begin{bmatrix} K + \frac{4}{3}G & K - \frac{2}{3}G & 0 \\ K - \frac{2}{3}G & K + \frac{4}{3}G & 0 \\ 0 & 0 & 2G \end{bmatrix} \tag{3.9}$$

and K and G are updated according to the current volumetric and deviatoric strain.

3.2 PW MODEL

The second model evaluated in this study, the PW model, was developed by the firm of Paul Weidlinger, Consulting Engineer, under a Waterways Experiment Station contract in connection with another project. The model is described in Reference 2 and, briefly, in Section 3.2.1 below.

3.2.1 Theory. The failure envelope in S_2 and P of most soils starts out as a straight line, but then flattens out and reaches a maximum with increasing pressure. Advanced plastic models mirror this behavior with a yield condition in which S_2 is taken as a more general function of pressure. (The JK model is of this general type.) In the PW model, the two pressure regions (i.e. the initial straight line and the portion after the curve begins to flatten) are represented by separate functions for the shear modulus.

The bulk modulus (K_{LD}) on loading is

$$K_{LD} = K_o + K_1 e + K_2 e^2$$

and for unloading is

$$K_u = K_{ou} + K_{1u} p$$

where K_o , K_1 , K_2 , K_{ou} , K_{1u} are appropriate curving constants and e is the mean volumetric strain

$$e = \frac{\varepsilon_{11} + \varepsilon_{22} + \varepsilon_{33}}{3}$$

For small pressure, i.e. for P less than some critical pressure P_c ,

$$G = \begin{cases} G_{LD} = G_o + \bar{\gamma}_1 \sqrt{S_2} + \gamma_1 p + \gamma_2 p^2 \quad , \quad \dot{S}_2 > 0 & (3.10) \\ G_{UN} = G_{oU} + \bar{\gamma}_{1U} \sqrt{S_2} + \gamma_{1U} p + \gamma_{2U} p^2 \quad , \quad \dot{S}_2 \leq 0 & (3.11) \end{cases}$$

where G_o , G_{oU} , γ_1 , γ_2 , $\bar{\gamma}_1$, γ_{1U} , γ_{2U} , and $\bar{\gamma}_{1U}$ are constants used

to fit the relations to the desired empirical curves. If $\gamma_1 > 0$ and $\gamma_2 < 0$ in Equation 3.10, then G_{LD} at constant S_2 will increase with increasing pressure until a maximum is reached at

$$P_c = -\frac{\gamma_1}{2\gamma_2} \tag{3.12}$$

If it is assumed that the same transition pressure P_c applies to both loading and unloading, then necessarily

$$\frac{\gamma_{1U}}{\gamma_{2U}} = \frac{\gamma_1}{\gamma_2} \tag{3.13}$$

For larger pressure, i.e. $P > P_c$,

$$G = \begin{cases} G_{LD} = G_1 + \bar{\gamma}_1\sqrt{S_2} \quad , \dot{S}_2 > 0 & (3.14) \\ G_{UN} = G_{1U} + \bar{\gamma}_{1U}\sqrt{S_2} \quad , \dot{S}_2 \leq 0 & (3.15) \end{cases}$$

Where:

$$G_1 = G_o - \frac{1}{4}\frac{\gamma_1^2}{\gamma_2} \tag{3.16}$$

$$G_{1U} = G_{oU} - \frac{1}{4}\frac{\gamma_1^2}{\gamma_2} \tag{3.17}$$

3.2.2 Application. For Cook's Bayou sand, the following constants were used to fit Equations 3.10 and 3.14 (unloading was not considered for the problem treated) to the constrained modulus curve in Figure 3.2:

$$G_o = 5.5 \times 10^3$$

$$\bar{\gamma}_1 = -4.5 \times 10^2$$

$$\gamma_1 = 3.6 \times 10^2$$

$$\gamma_2 = -3.9 \times 10^{-2}$$

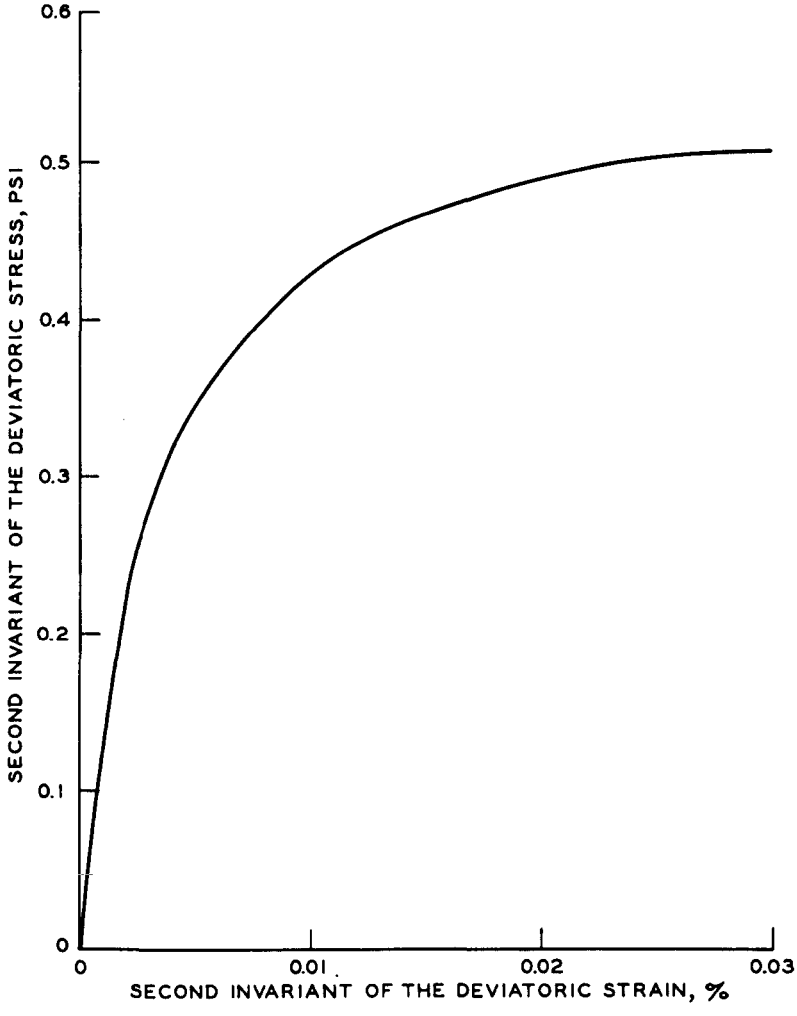

Figure 3.1 Limiting shear behavior of the JK soil model for P = 0 .

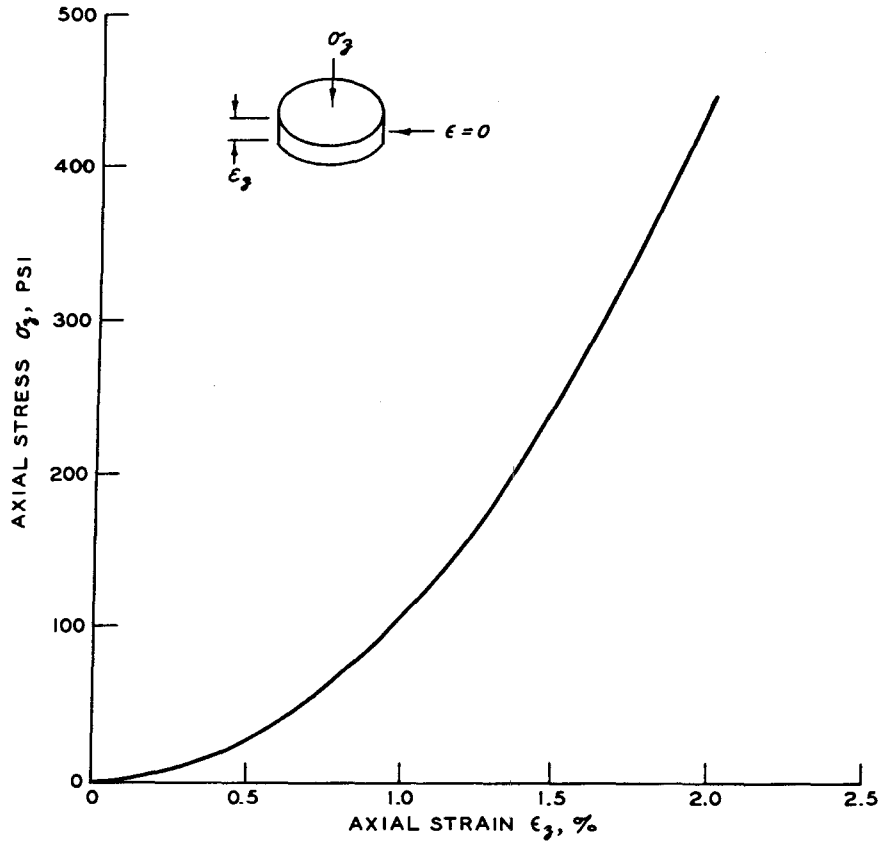

Figure 3.2 Constrained modulus M test for Cook's Bayou sand.

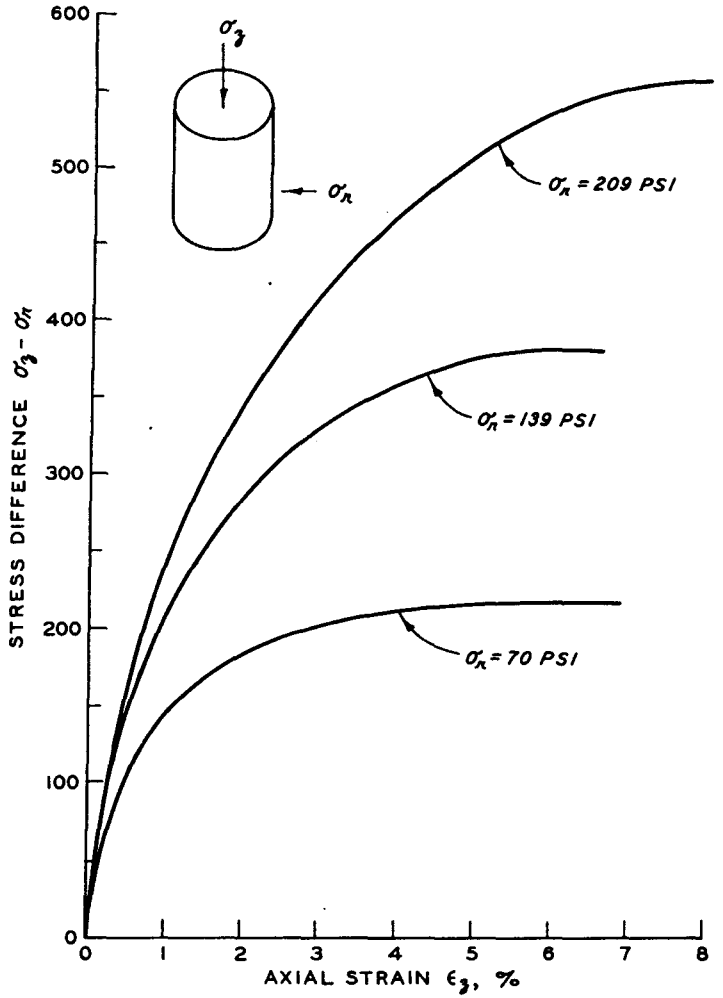

Figure 3.3 Triaxial compression test for Cook's Bayou sand.

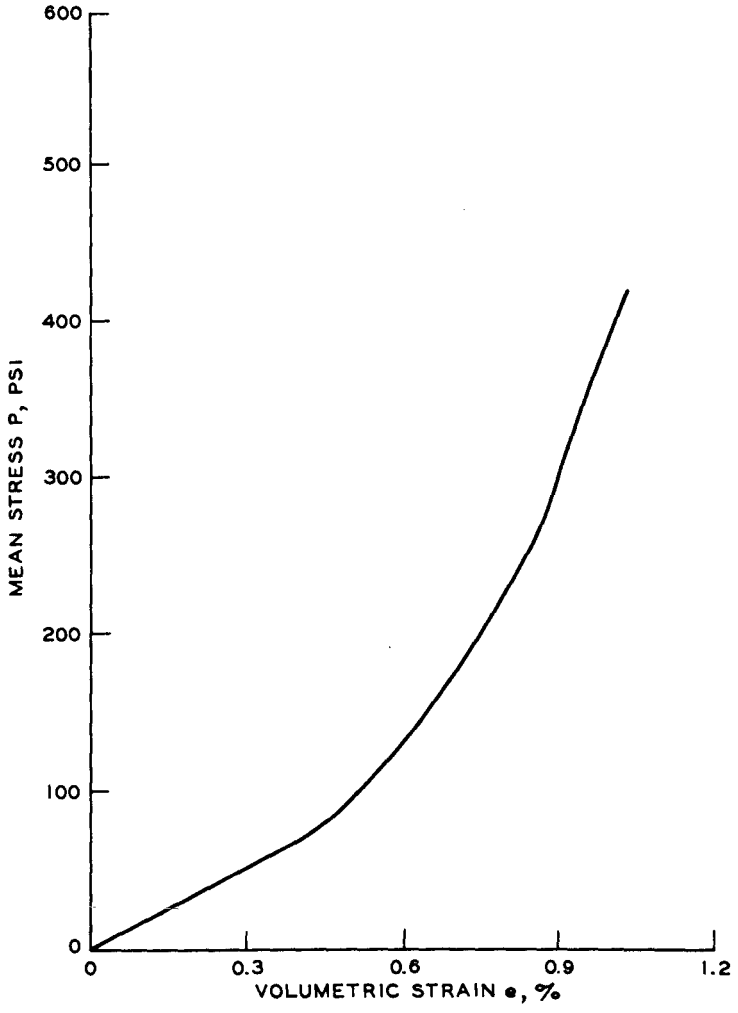

Figure 3.4 Calculated pressure-volume curve for Cook's Bayou sand, JK model.

CHAPTER 4

COMPUTER CODE

The code is written with a dynamic storage allocation; i.e., all variables whose sizes are dependent on the problem being solved are stored in a large, one-dimensional array in the blank common. The size of this array may be adjusted depending on the capacity of the computer being used, and, for smaller problems, a reduced field length may be specified which will truncate the blank common in order to reduce the computer storage.

In working any problem with the code, a sequence of events is followed. The flow sequence of the computer code is indicated in Figure 4.1. The following is a brief description of the functions of the subroutines used in the computer code.

SIGEPS analyzes the current values of the volumetric strain and second invariant of the deviator strain and assigns K and G values to be used in Equation 3.1. Once K and G have been determined, STIFF is used to form the stiffness matrix for the element under consideration and embed the element stiffness in a large array that has been set aside for the stiffness of the entire system of elements. LOAD increases the load on the system, and BACKS finishes the solution to the equations expressing equilibrium for this incremental problem.

The strains resulting from the displacements are calculated in STRAIN as shown in Loop 1 in Figure 4.1, and Loop 1 is cycled for each element of the system. Once every element has been cycled through Loop 1, the system stiffness for this increment of the problem has been formed, and subroutine TRIA in Loop 2 triangularizes the big matrix. LOAD sets a new load increment, and the procedure is repeated until all load increments have been cycled.

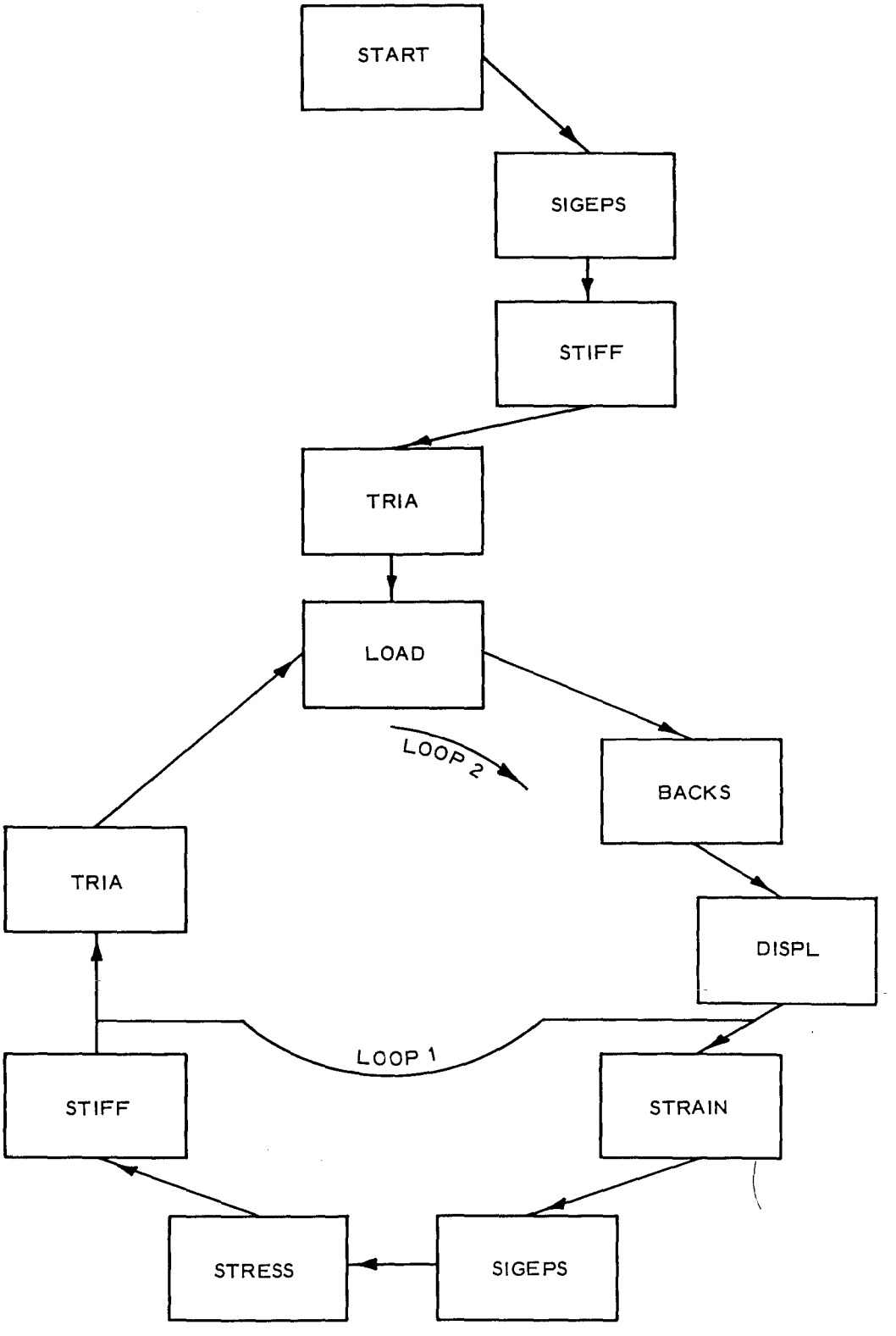

Figure 4.1 Program flow diagram.

CHAPTER 5

EXPERIMENTAL PROGRAM

As part of a study of the response of stiff cylinders, static tests were conducted on buried cylindrical shells constructed from 6-inch-outside-diameter steel pipes. Wall thicknesses used in the tests were 1/8, 1/4, and 3/8 inch, as can be seen in Figure 5.1. By testing a specimen of the steel cylinder, Young's modulus was determined to be 29.5×10^6 psi. The sand used in the tests was Cook's Bayou sand, a local fine-grained sand whose characteristics were described in Chapter 3.

The test geometry was designed so that the central test section of the buried cylinder was isolated from the closed ends as shown in Figure 5.2. The Small (4-foot-diameter) Blast Load Generator (SBLG) at the WES was used in testing the buried cylinder. Figure 5.3 gives a cross-section elevation view of the test geometry and shows how the boundary value problem which was solved by the computer code fits into the test geometry.

A double polyethylene liner with a greased interface was attached to the wall of the SBLG to reduce the wall friction. Because of the high lateral stiffness of the SBLG wall, a zero-displacement boundary condition was used in the finite element model as indicated in Figure 5.3. Much care was taken to insure that the test section of the cylinder was buried in the sand so that the symmetry indicated in Figure 5.3 was maintained (Reference 16). It is assumed that the testing arrangement provides a condition of plane stress along the axis of the buried cylinder.

Strain measurements were recorded on the test section on both the inside and outside surfaces at 30-degree intervals around the cylinder. Vertical and horizontal stress components were recorded within the sand by means of a wafer-type diaphragm soil pressure transducer located 6 inches from the outer wall of the test cylinder and at an elevation corresponding to the middepth of the structure. The static overpressure was monitored by pressure gages mounted in the loading bonnet of the test chamber.

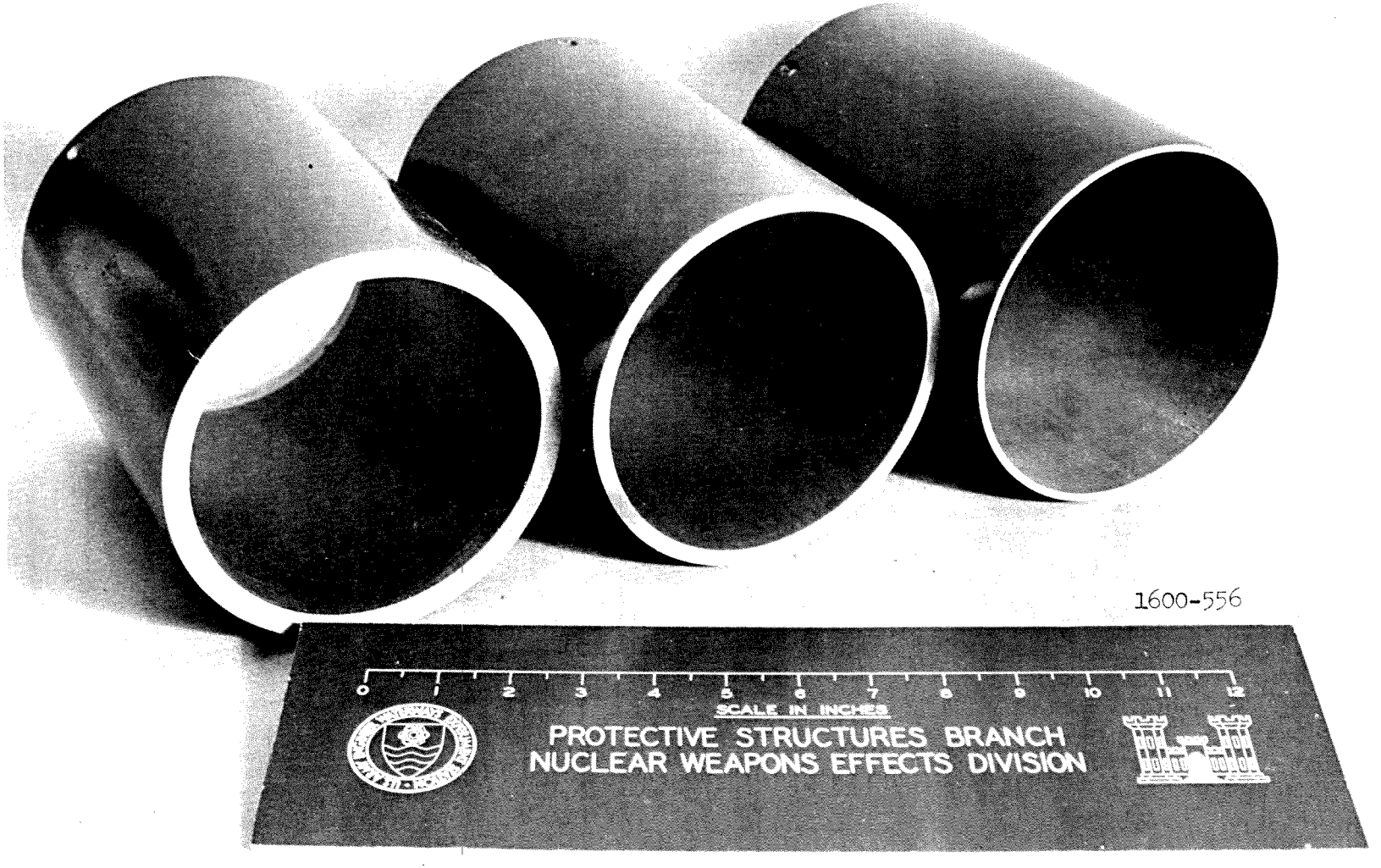

Figure 5.1 Comparison of cylinder thicknesses.

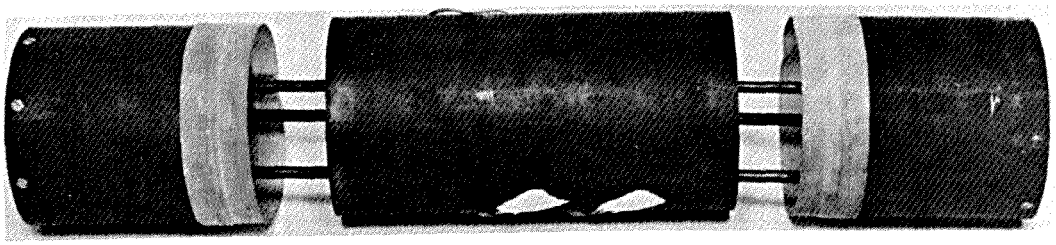

a. EXPLODED VIEW

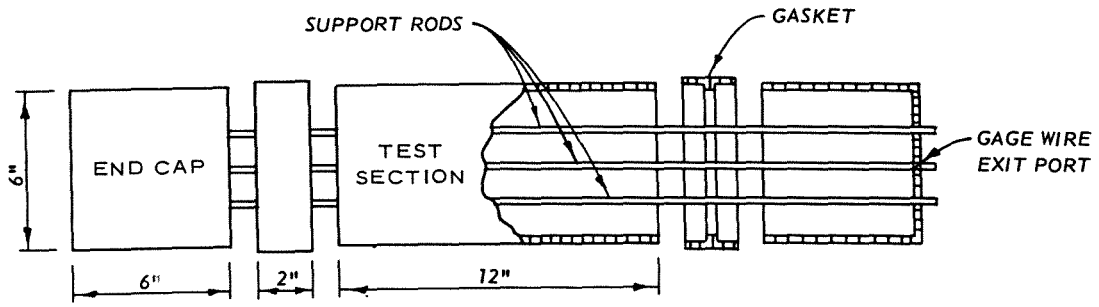

b. GEOMETRY

Figure 5.2 Exploded view and geometry of test structure.

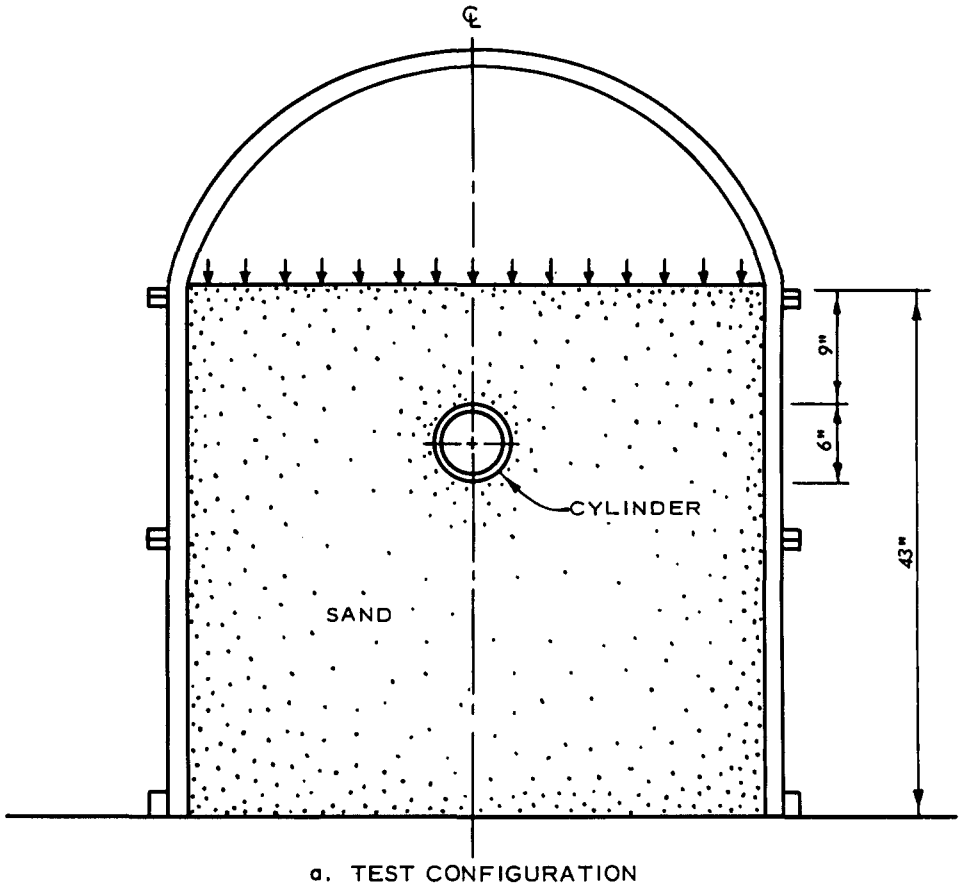

a. TEST CONFIGURATION

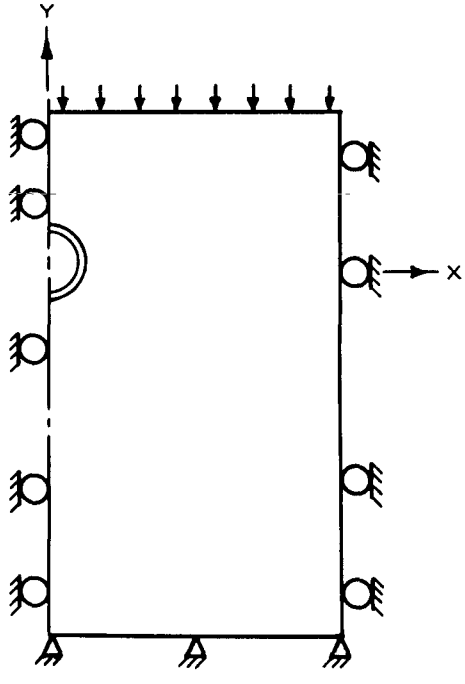

b. BOUNDARY CONDITIONS

Figure 5.3 Test configuration and corresponding plane boundary value problem.

CHAPTER 6

RESULTS

As discussed in Chapter 3, the approach used in this study to include the physical nonlinearities of the soil medium adds a succession of linear incremental problems. For the incremental problems, each element is assigned linearly elastic constants based on the current states of stress and strain that exist in that element. As one should expect, this type of detailed analysis is costly computerwise. For instance, in the following results for the JK model, 50 incremental problems were used for each cylinder configuration, requiring approximately 21 minutes of Univac 1106 computer time.

For solution, the boundary value problem described in Figure 5.3b was partitioned into 314 elements using 347 node points as shown in Figure 6.1. The cylinders are represented in the finite element idealization using two elements to span their wall thicknesses.

6.1 JK MODEL

6.1.1 Free-Field Response. In Figures 6.2, 6.3, and 6.4, the stress components measured in the soil are compared with the calculated stress components at the same locations. Several of the soil pressure gages did not operate during the tests, and thus their comparison plots are missing. The agreement between the calculated and measured values (especially for the 3/8-inch cylinder) is an indication that the equivalent continuum model is representative of the soil insofar as the free-field stress components are concerned.

6.1.2 Deflection. Figure 6.5 shows a comparison of the values of the change in vertical diameter ΔD calculated by the JK model with the experimental values for each of the three cylinders. As can be seen, the calculated values consistently fall somewhat below those measured in the experiment. Good agreement is indicated for the 3/8-inch cylinder, but the agreement lessens for the thinner cylinders.

6.1.3 Moment. Figures 6.6 and 6.7 indicate the moments developed

in the cylinders at the crown (0 degrees) and the invert (180 degrees), respectively. The discrepancies in these graphs are consistent with the deviations between calculated and measured deflections displayed in Figure 6.5; i.e. calculated momemts are consistently lower than the experimental values and agreement is better for the thicker cylinder.

6.1.4 Thrust. Figures 6.8 and 6.9 are thrust comparisons for the crown and invert, respectively. Thrusts at the invert are generally in fair agreement with the calculations except for the higher pressure response of the 3/8-inch cylinder. Thrusts at the crown, except for the 1/8-inch cylinder, show a wide discrepancy. The experimental thrust calculation involves taking the difference of two recorded strain measurements, and this accounts for the erratic variations of the thrust curves. The experimental measurements indicate that very little thrust developed at the crown of the thicker cylinders. Even though the oscillation in the experimental thrust curves indicates scatter in the data, it is felt that the curves reflect global behavior of the thrusts.

6.2 PW MODEL

The PW model was employed to demonstrate the flexibility of the computer code and to test the possibility that this more sophisticated soil model might yield better agreement with experimental results than the JK model.

Since the calculations described in Section 6.1 have demonstrated the utility of the computer code and defined the problem areas of the JK model, only a limited number of calculations are presented for the PW model to demonstrate its accuracy in relation to the JK model.

As shown in Figure 6.10, results for vertical diameter change are very nearly the same for the two models, with only slightly better agreement with experimental results being demonstrated by the PW model. Similar results are shown for moment at the crown in Figure 6.11.

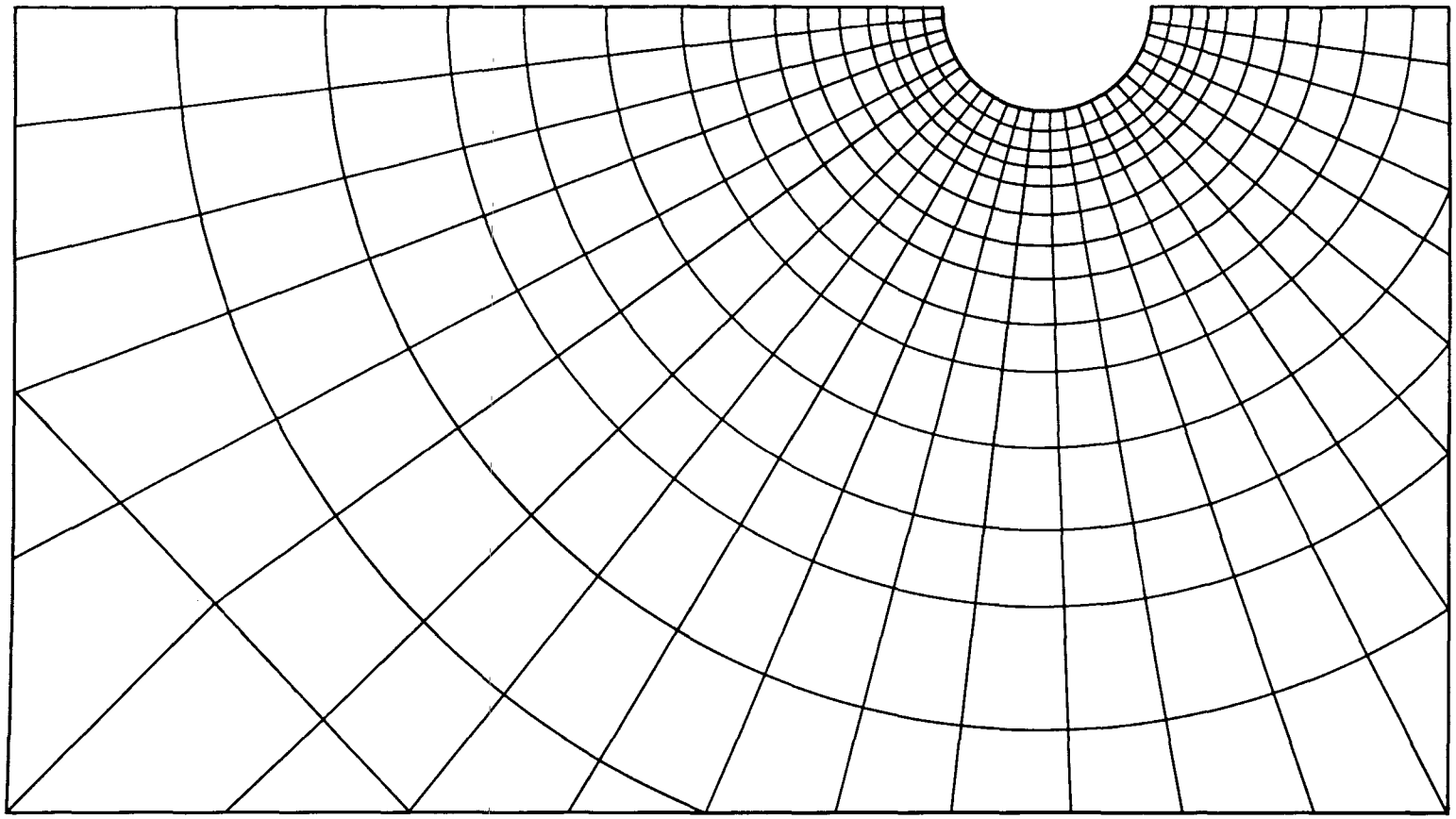

Figure 6.1 Finite element idealization of the buried cylinder configuration.

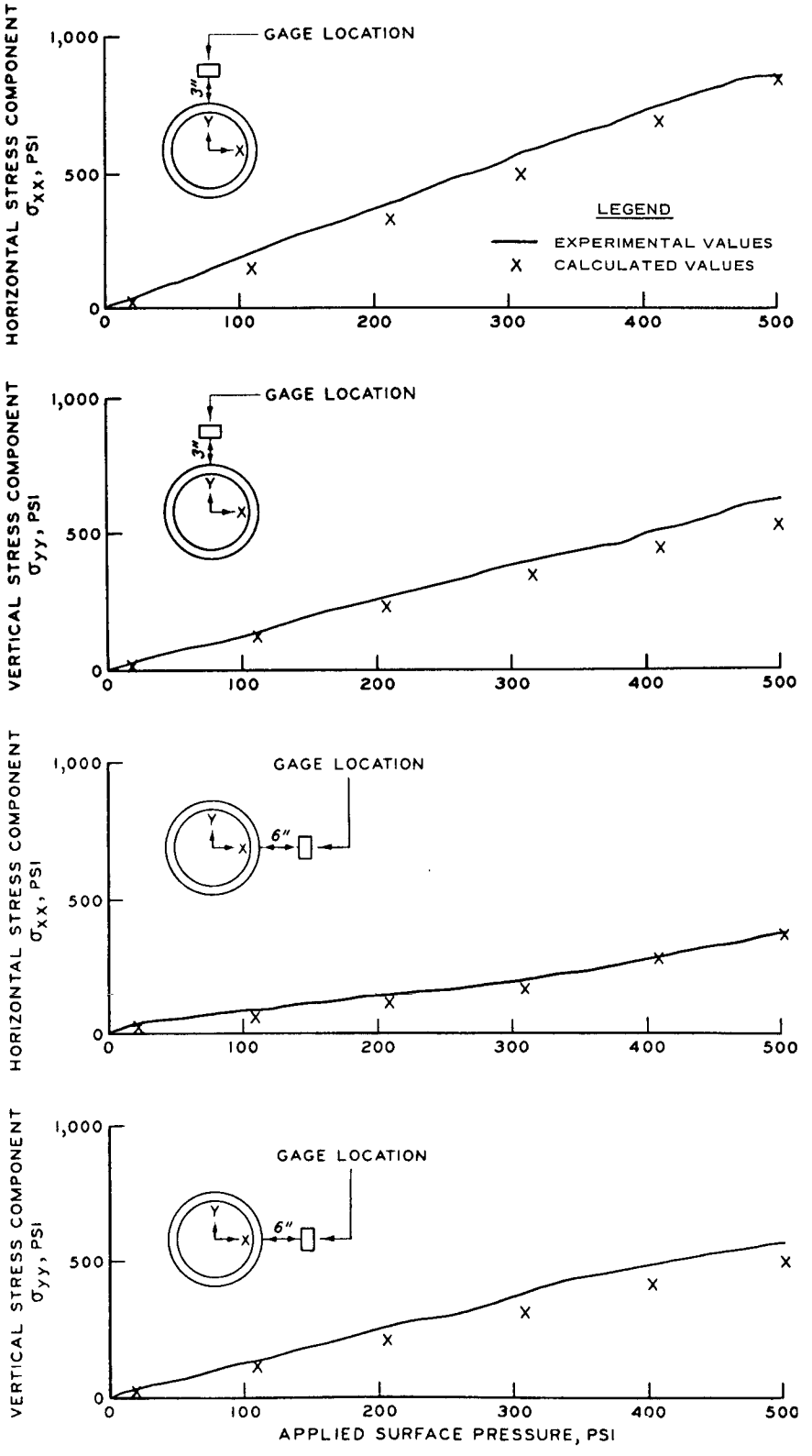

Figure 6.2 Comparison of experimental and calculated stress components for 3/8-inch cylinder.

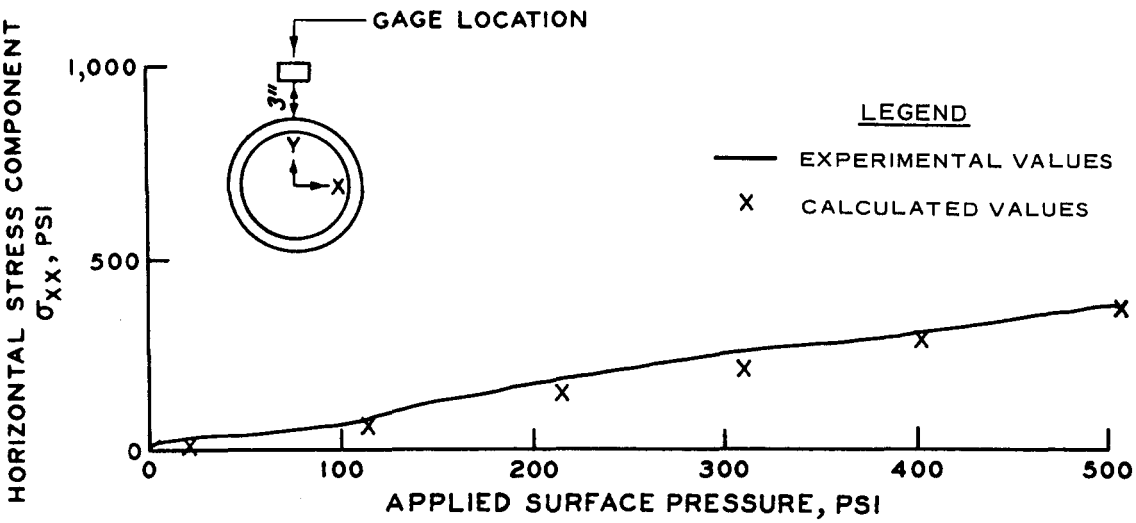

Figure 6.3 Comparison of experimental and calculated stress components for 1/4-inch cylinder.

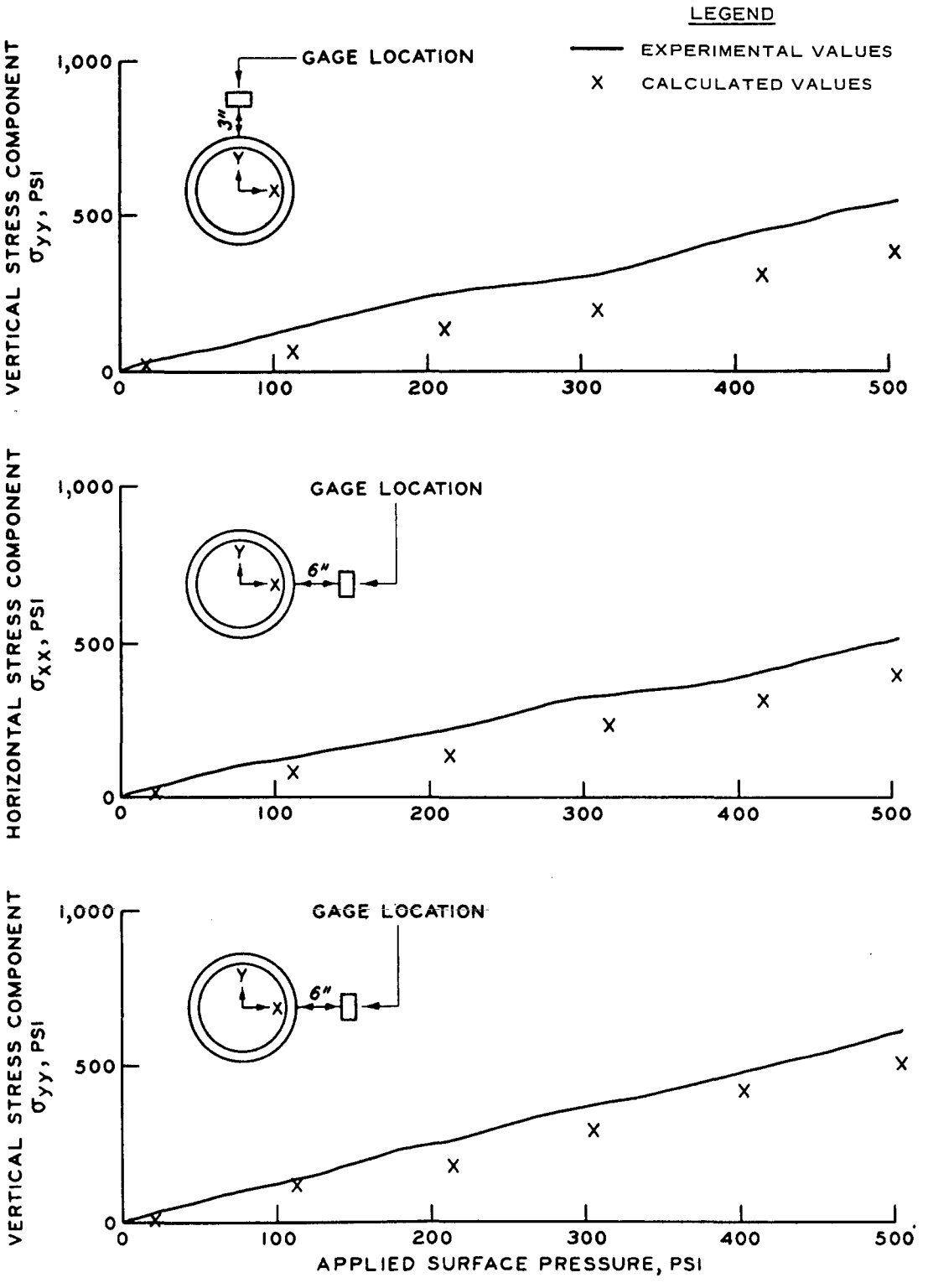

Figure 6.4 Comparison of experimental and calculated stress components for 1/8-inch cylinder.

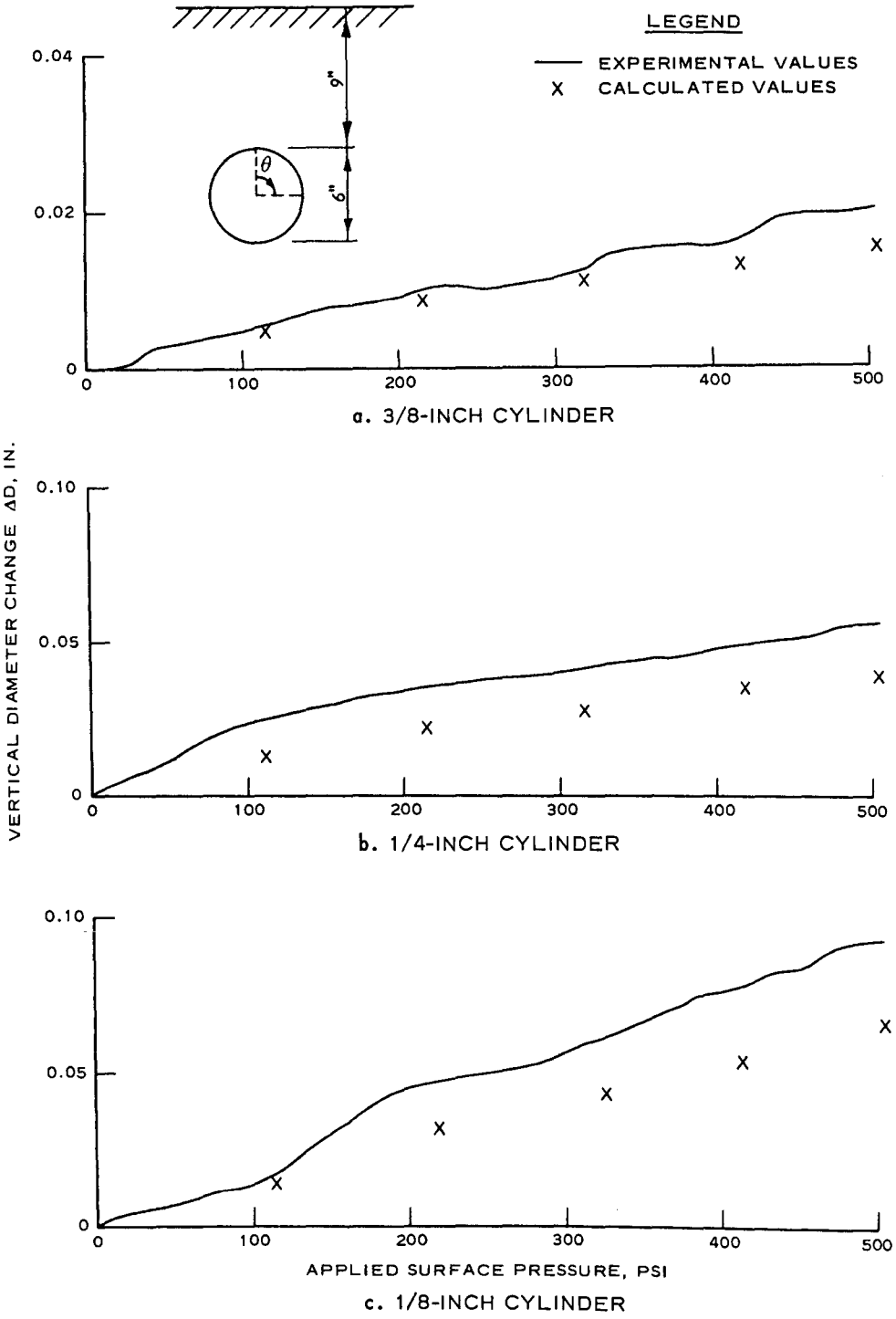

Figure 6.5 Comparison of experimental and calculated diameter changes.

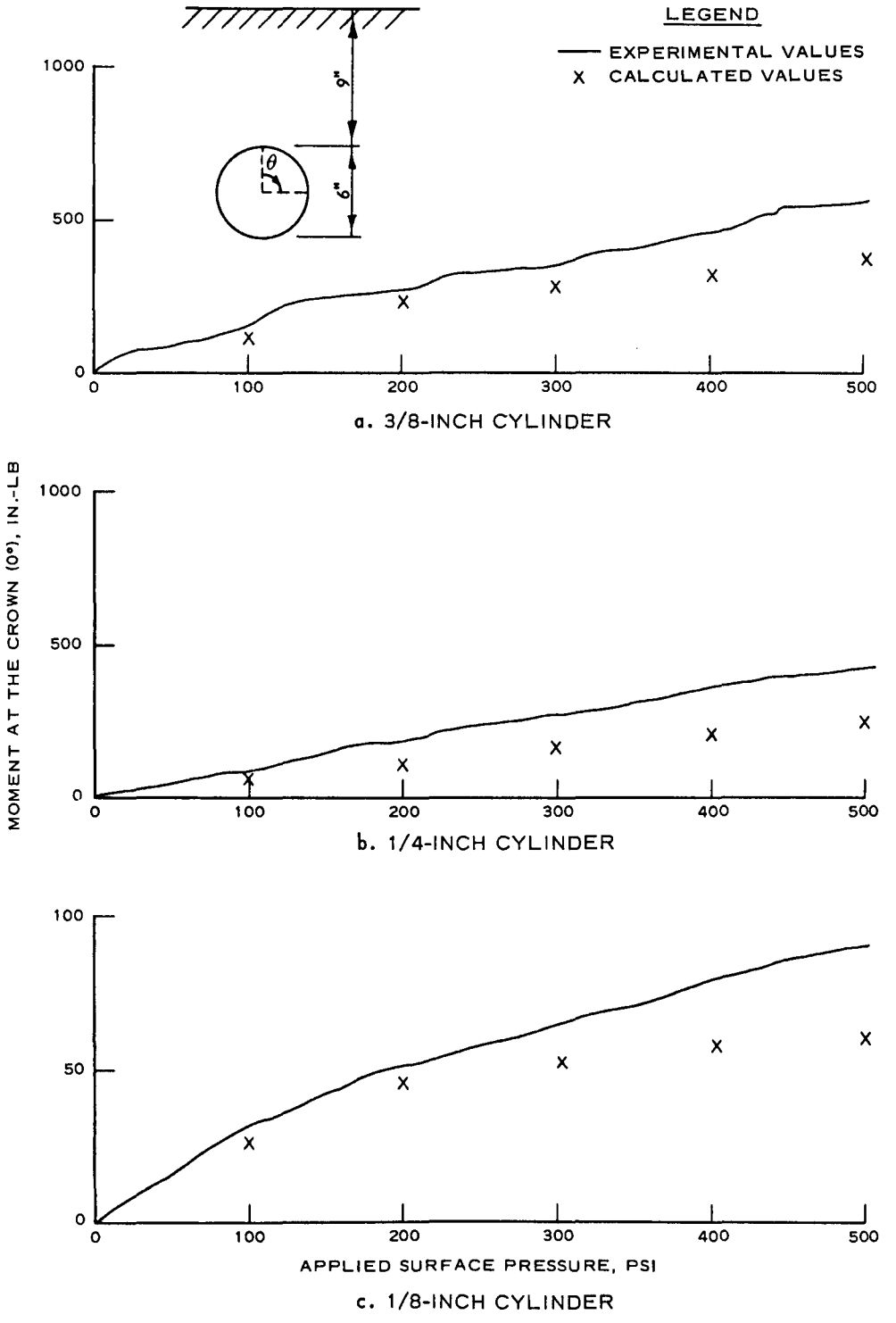

Figure 6.6 Comparison of experimental and calculated moments at the crown.

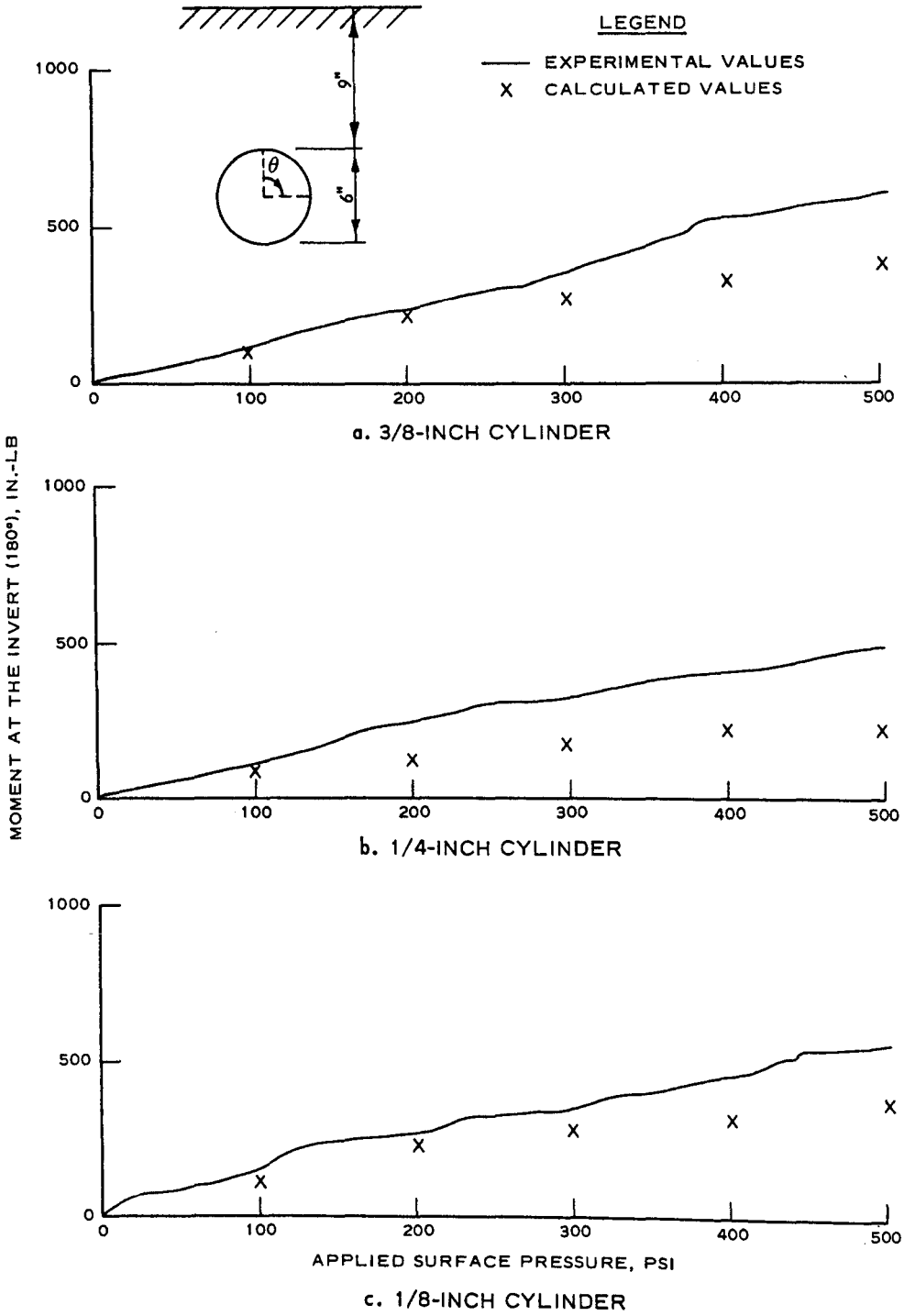

Figure 6.7 Comparison of experimental and calculated moments at the invert.

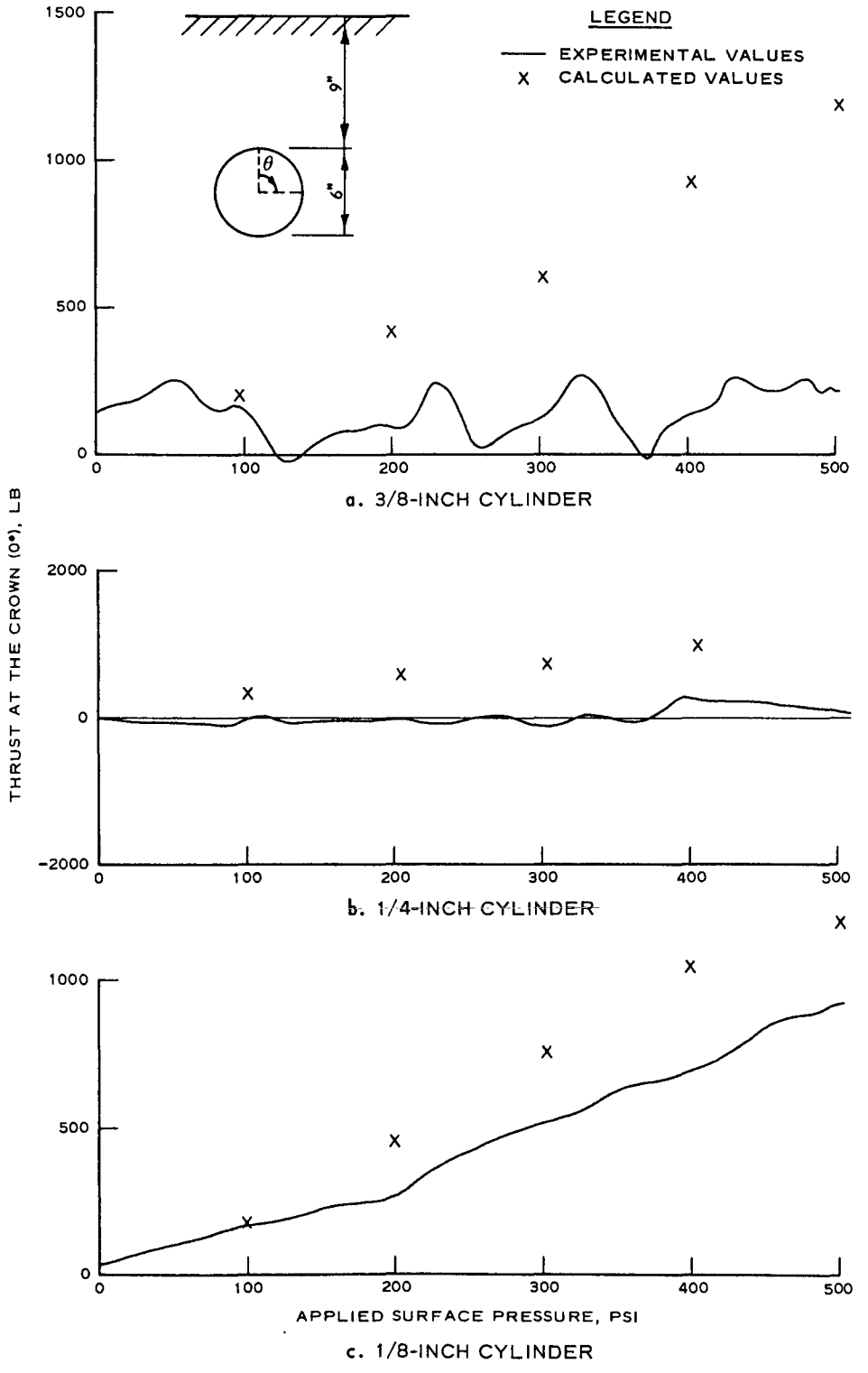

Figure 6.8 Comparison of experimental and calculated thrusts at the crown.

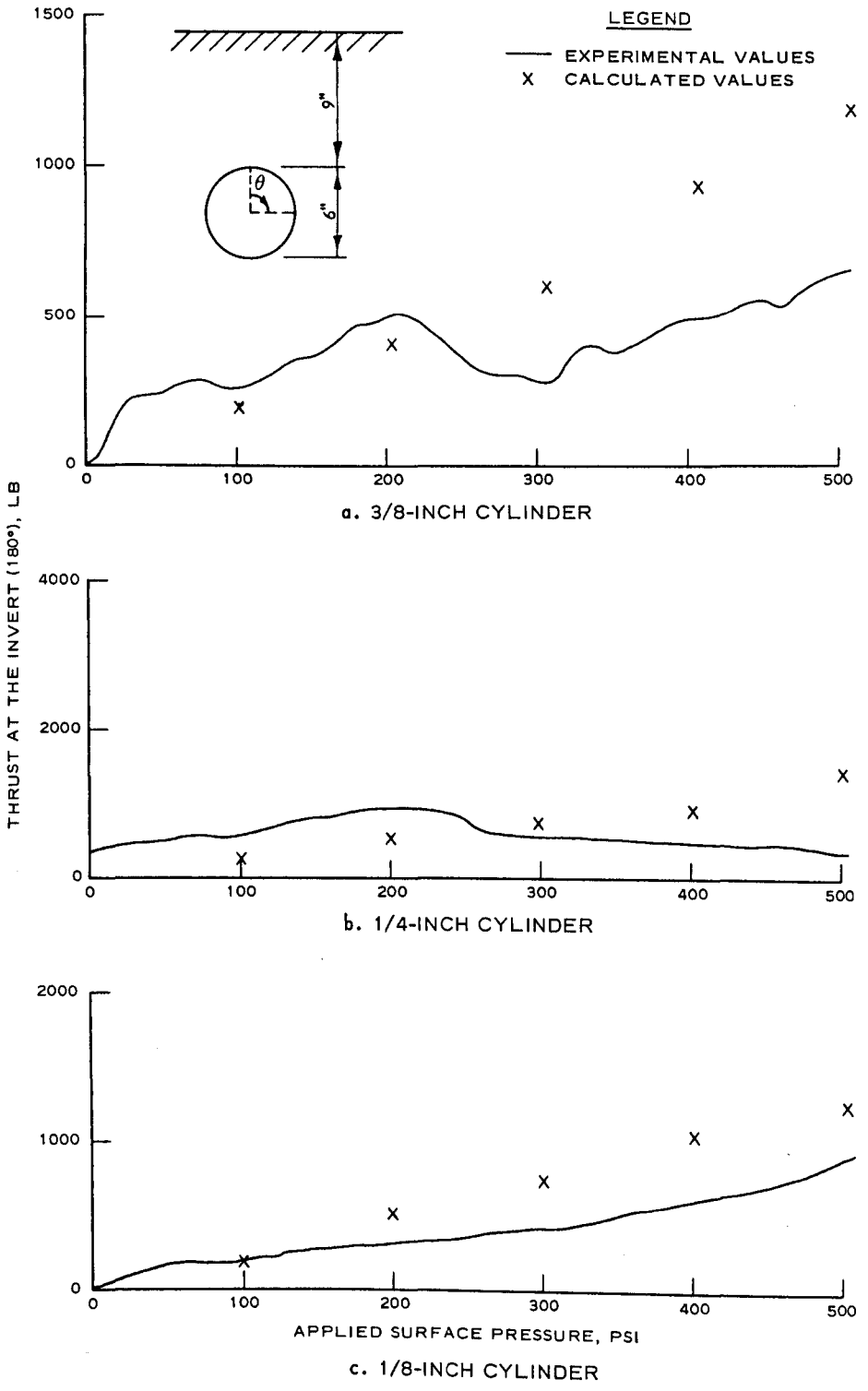

Figure 6.9 Comparison of experimental and calculated thrusts at the invert.

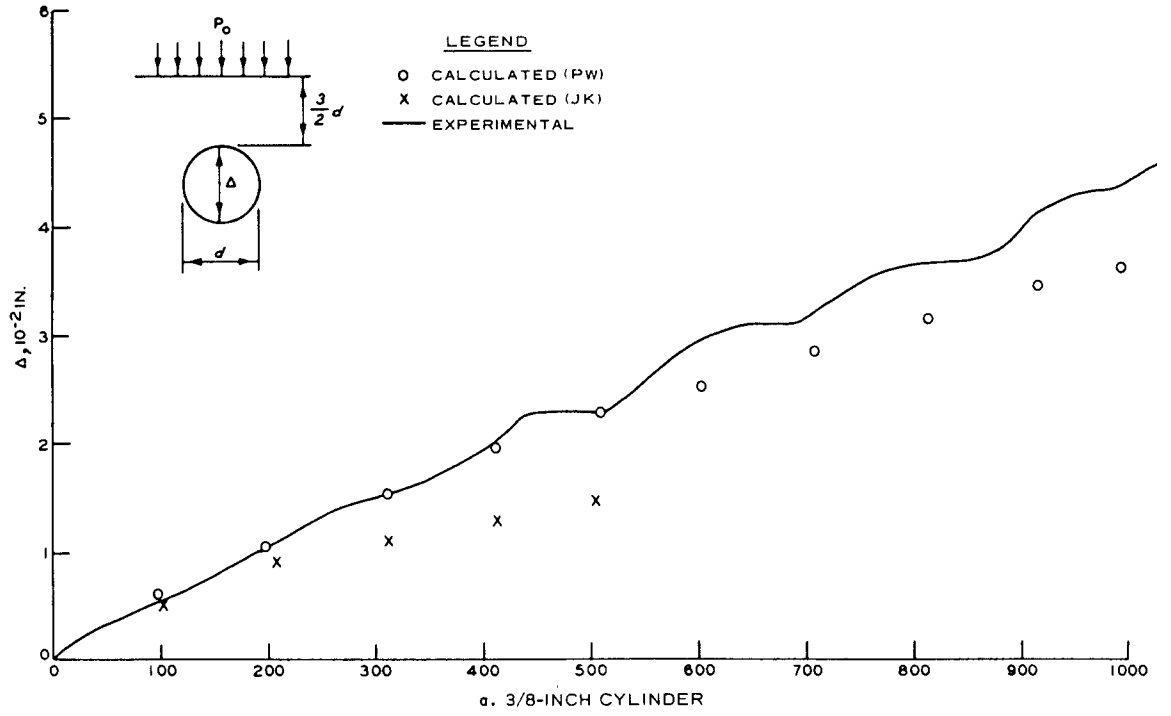

a. 3/8-INCH CYLINDER

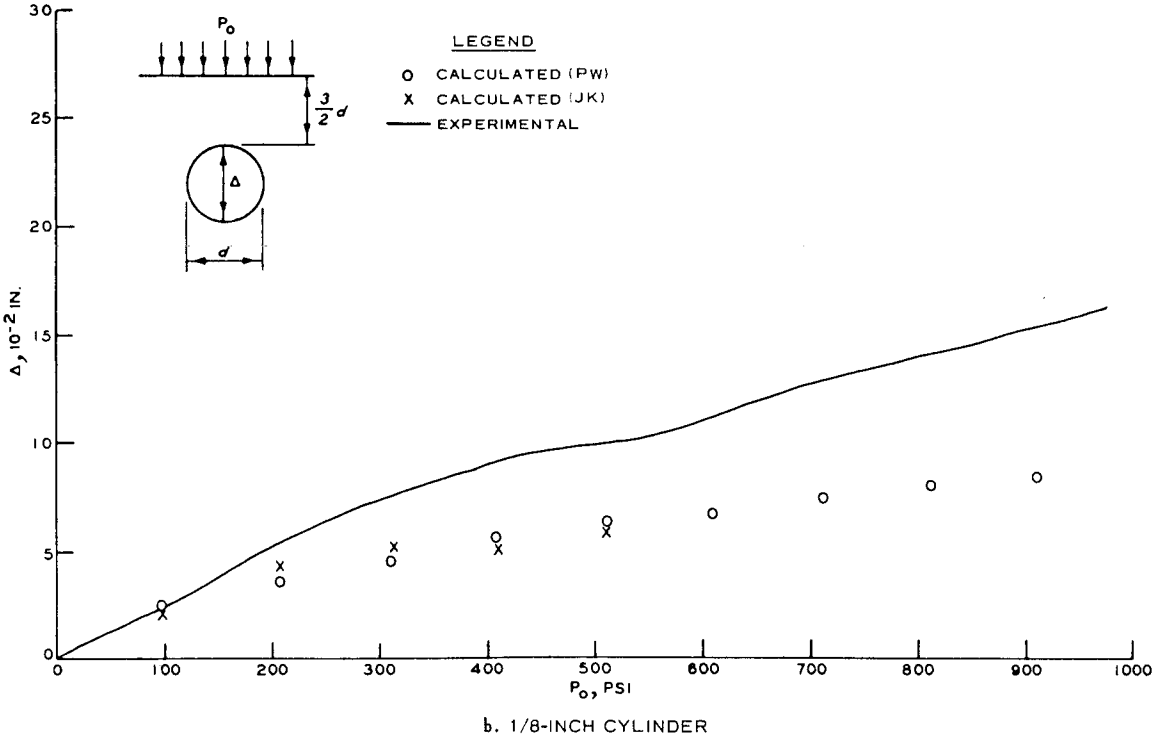

b. 1/8-INCH CYLINDER

Figure 6.10 Comparison of JK and PW model calculations with experimental diameter change.

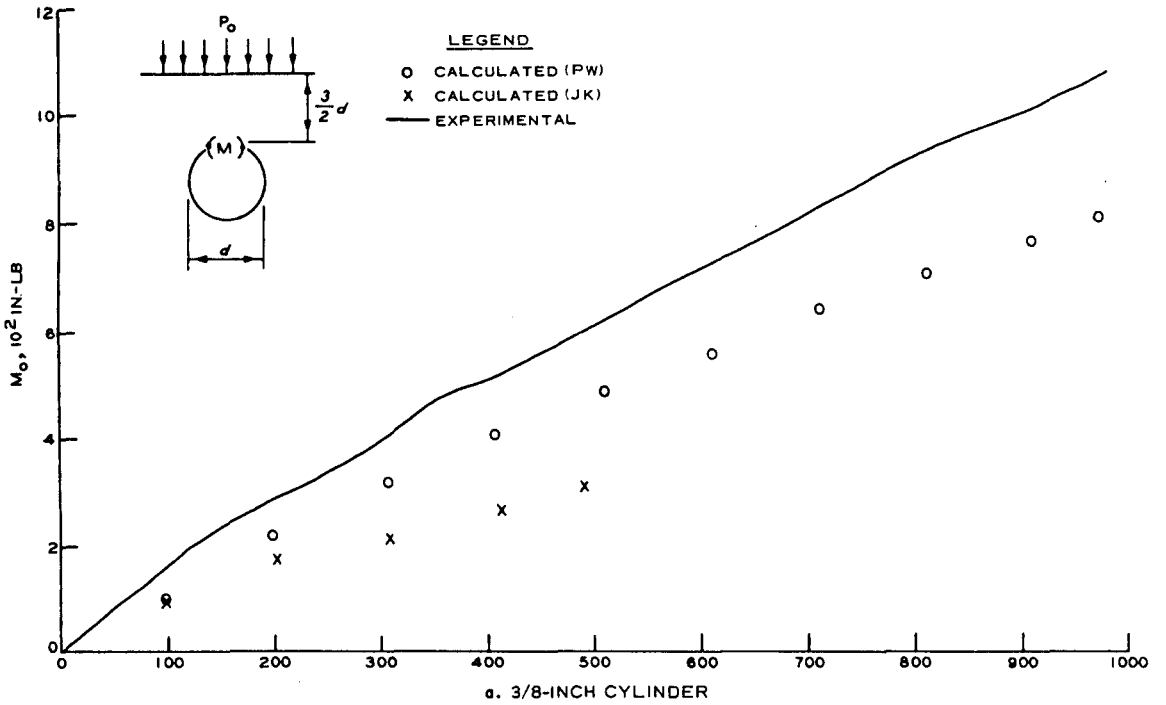

a. 3/8-INCH CYLINDER

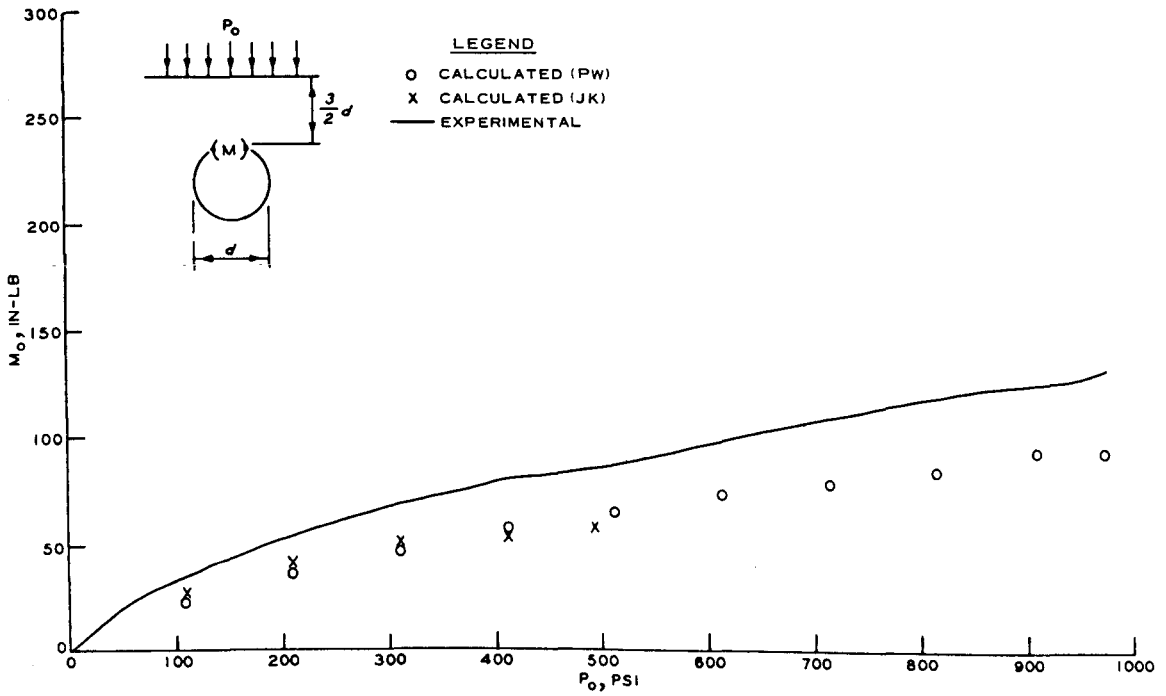

b. 1/8-INCH CYLINDER

Figure 6.11 Comparison of JK and PW model calculations with experimental moment at the crown.

CHAPTER 7

DISCUSSION OF RESULTS

Although the geometry involved in this study is not complex, the nature of the problem was such that it presented a meaningful test of the soil-structure interaction code. The variation in the stiffness of the cylinders tested was sufficient to include cases of active arching (the structure carries less load proportionally than the surrounding soil) and passive arching (the structure carries more load proportionally than the surrounding soil). Thus, as discussed in the following section, the loading conditions of the soil in the vicinity of the cylinders differed significantly from the 3/8-inch- to the 1/8-inch-thick cylinder.

7.1 STRUCTURAL RESPONSE

Using the JK model, the deformed shapes of the cylinders were calculated by subtracting out the rigid body motion of the cylinder (Figure 7.1). Only the vertical diameter change was measured in the experiment, and the recorded data points are indicated in the figure. The deformation patterns are substantially as one would expect under the loading conditions.

The calculated deflections of the soil surface for the three cylinder configurations are shown in Figure 7.2. These curves are indicative of the relative stiffness of the cylinders as compared to the soil model.

Figure 7.3 contains comparisons of the vertical stresses at the crown with the horizontal stresses at the spring line in the soil elements which are adjacent to the cylinder. These graphs further illustrate the stiffness of the cylinders relative to that of the soil: the 3/8-inch cylinder giving σ_{yy} at the crown greater than σ_{xx} at the spring line; the 1/4-inch cylinder showing the two stress components to be relatively close together; the 1/8-inch cylinder having σ_{xx} at the spring line greater than σ_{yy} at the crown.

7.2 DEGREE OF CORRELATION

The computer code developed and the two soil models employed generally yielded a fair approximation of the structural response of the cylinders tested. Free-field response of the soil was reproduced with good accuracy. Deflections were generally underpredicted by the code, but calculated values were reasonably close to those measured. Moments and thrusts were not as accurately predicted as deflections, and for the stiffer cylinders, there were significant discrepancies.

There are several indications that the environment of the cylinders in the model was different from that in the test. For instance, the recorded free-field components of stress are in reasonable agreement with the calculated values, but experimental values of thrust at the crown of the 3/8-inch cylinder indicate that it received essentially no lateral support from the soil at these pressure levels. On the other hand, the experimental values of thrust at the crown of the 1/8-inch cylinder indicate that it received lateral support from the soil.

The most probable explanation for these discrepancies seems to be an area of reduced density in the soil below the spring line and adjacent to the cylinder. Although sophisticated placement techniques were employed for the tests, it is very difficult to obtain a uniform backfill, especially in this region. And, as discussed in the next paragraphs, the stiff cylinders would be very sensitive even to relatively small differences in density in this region.

Figure 7.1 indicates the different magnitudes of displacement experienced by the soil in the region of the spring line of the cylinder. The stiff cylinder deflected very little at the spring line and thus would have derived very little support from the surrounding soil due to the reduced density zone. However, the relatively flexible cylinder experienced a deflection at the spring line that would mask the reduced density zone. Of course, if the compression mode of the cylinder is not mobilized, the load must be carried as moment. Thus the moment would be greater than expected in such cases. As indicated by Figure 6.6, this

is apparently the situation that developed in the experiments considered in this analysis.

If the hypothesized reduced density zone exists, it is doubtful if any prediction scheme which uses a homogeneous soil model will be completely successful for very stiff cylinders. The values of the moments and thrusts which develop in stiff cylinders are very sensitive to the immediate soil environment of the cylinder because of the small deformation of the cylinder-soil interface. Thus, irregularities which are masked by the larger deflection associated with the flexible cylinders become extremely important for stiff cylinders.

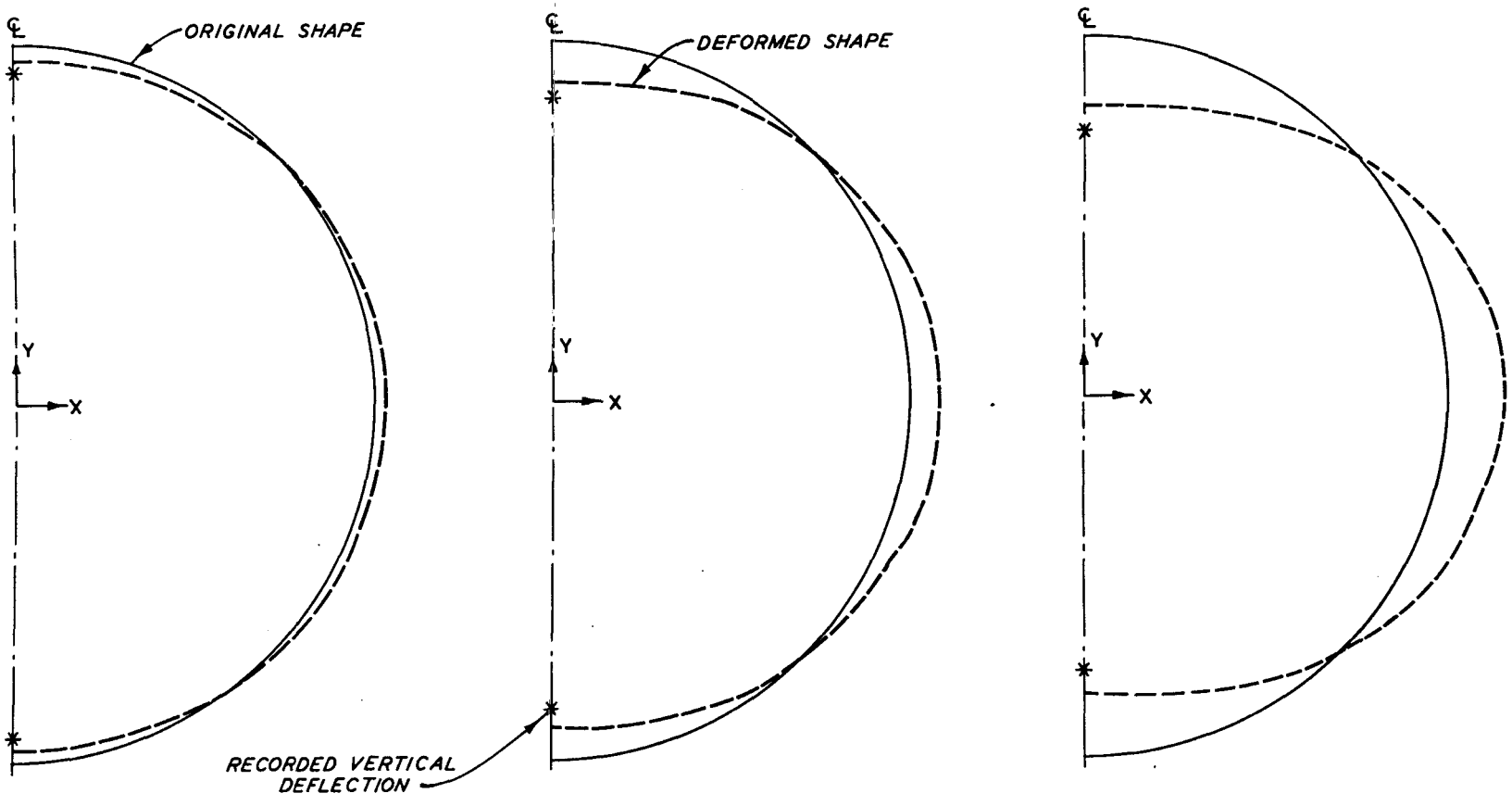

a. 3/8-inch cylinder. b. 1/4-inch cylinder. c. 1/8-inch cylinder.

Figure 7.1 Deformation patterns.

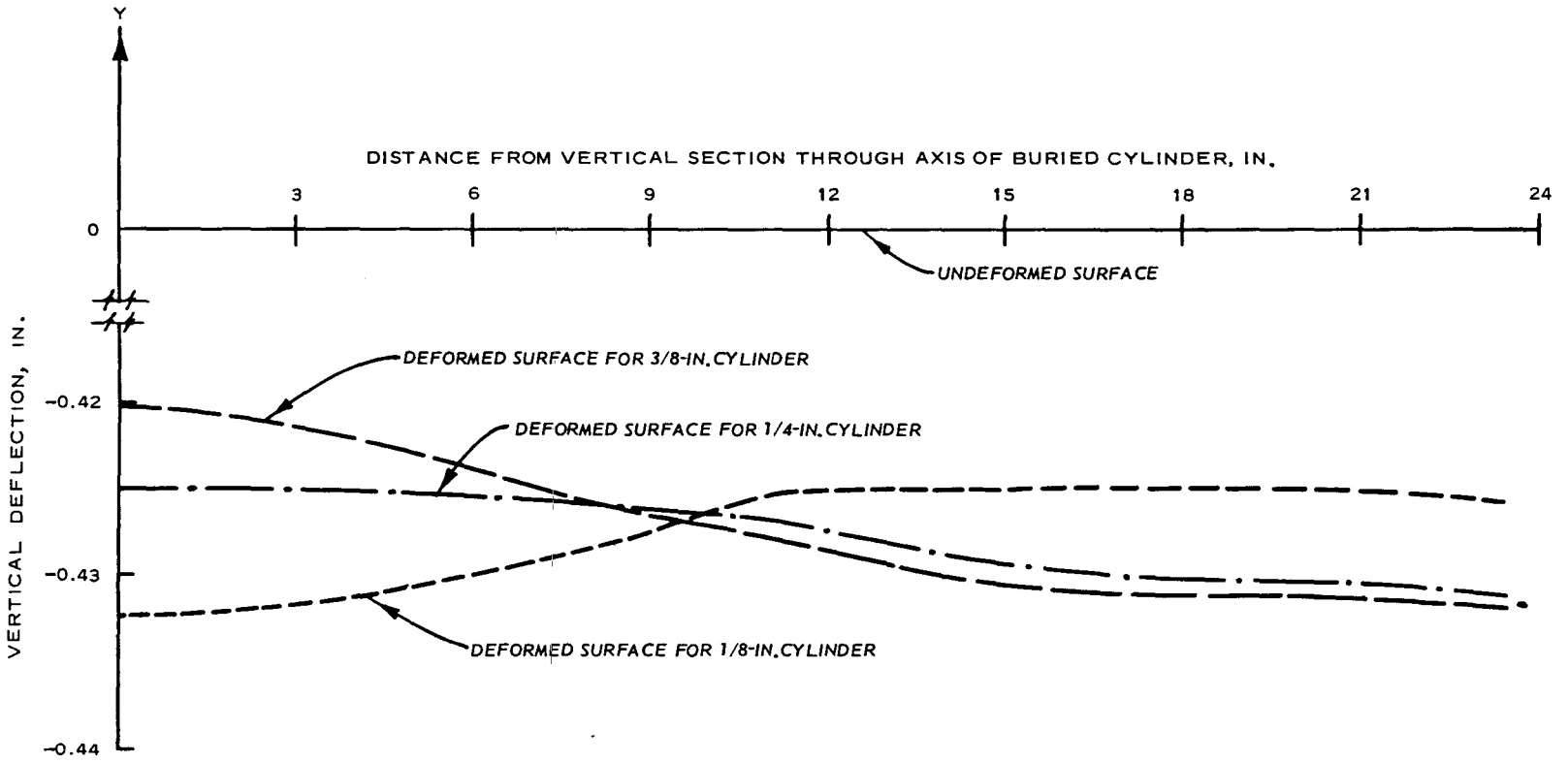

Figure 7.2 Soil surface deflections.

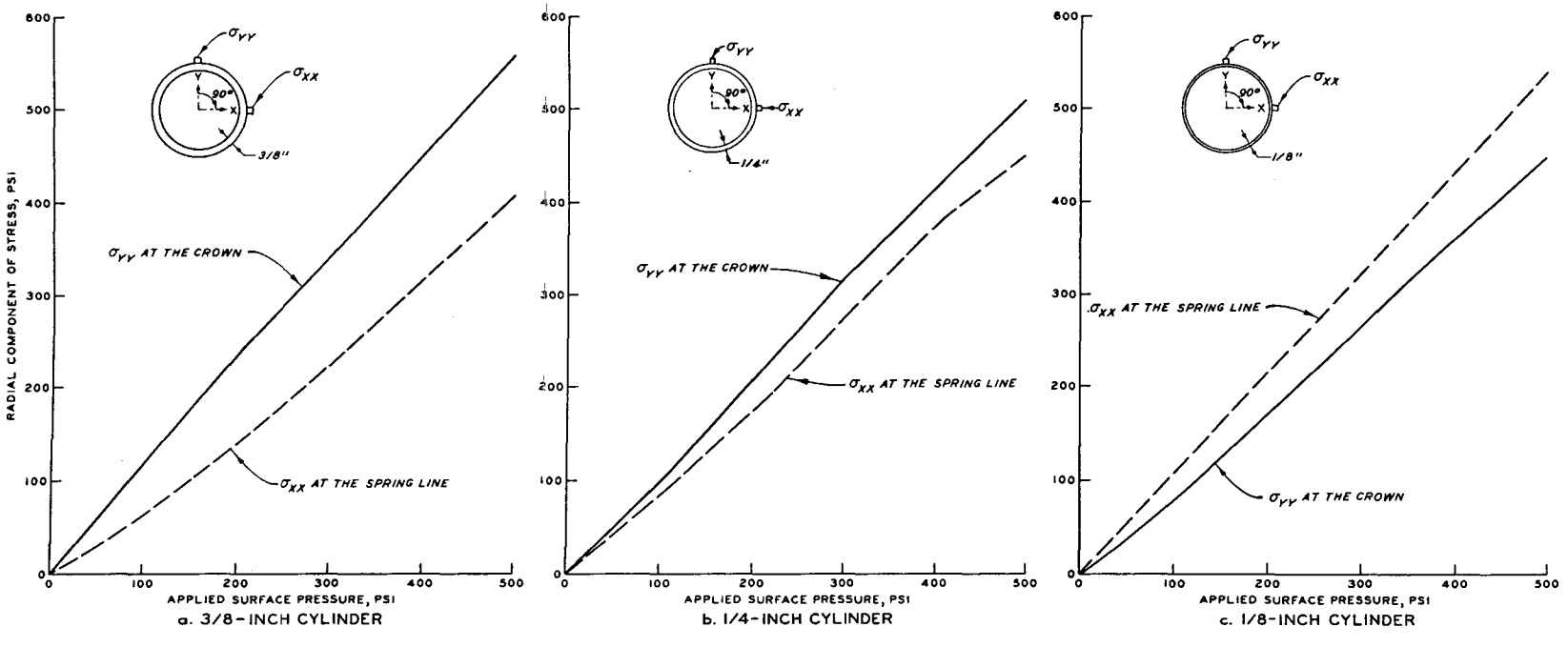

Figure 7.3 Comparison of the radial stresses at 0 and 90 degrees.

CHAPTER 8

CONCLUSIONS AND RECOMMENDATIONS

Inherent characteristics of the finite element procedure make it applicable to arbitrary geometries, arbitrary loadings, and inhomogeneous medium problems. This type of numerical procedure is especially suited to problems where there is a need to take into account the soil-structure interaction effects. In many of the earlier efforts, the effects of the interaction phenomenon were generally neglected, or some crude model with springs representing the interaction effects of the soil was used. In the finite element representation of the system, the interaction effects are included automatically, and thus a more realistic treatment of the problem is possible.

Although the geometry involved in this study was not complex, the nature of the problem was such that it presented a meaningful test for the soil-structure interaction code. The stiffness of the cylinders involved varied sufficiently to cover both active and passive arching. Thus the loading conditions of the soil in the vicinity of the cylinders differed significantly from the 3/8-inch- to the 1/8-inch-thick cylinder.

The computer code developed and the two soil models employed generally represent a reasonable method for predicting the response of buried cylinders, and undoubtedly other geometries as well. Free-field response of the soil was reproduced with good accuracy. Deflections were generally underpredicted by the code, but calculated values were reasonably close to those measured. Moments and thrusts were not as accurately predicted as deflections, and for the stiffer cylinders, there were significant discrepancies.

The nature of the discrepancies between experimental and calculated results indicates that lateral support of the cylinders did not develop in the experiments. Thus, in the experiments, the cylinders responded in essentially a flexural mode, whereas the finite element calculations developed a lateral load consistent with the uniform soil model assumed

for the analysis. It should also be noted that both soil models gave very similar structural responses.

Analysis of stiff cylinders is confounded by the fact that a detailed knowledge of the interface zone is needed, and, yet, this is the region about which the least is known. Meaningful measurements in this region are difficult to obtain.

One method of attack on such problems would be to consider a region below the spring line and adjacent to the cylinder (the region where the sand placement is most difficult) as a material with properties different from the other sand. By making computer calculations using such a heterogeneous soil model, the influence of a reduced density zone could be varied in subsequent computer calculations in an attempt to obtain the experimental values for moment and thrust.

If it is possible to determine a heterogeneous soil model which predicts the high moment and low thrust response measured in these experiments, the same scheme can be examined for buried structures of other shapes. By extending the investigation to cylinders of larger diameter, perhaps the normal component of stress can be measured around the cylinder, giving an experimental indication of the value of the lateral load on the buried cylinders. Therefore, it is recommended that future effort be directed along this approach.

APPENDIX A

DERIVATION OF SHEAR MODULUS

The idea of a limited shear may be made a property of the mathematical model by considering the inner energy ϕ_2 as

$$\phi_2 = -2\sqrt{\bar{\sigma}}\left[\sqrt{-I_2'} - \frac{\sqrt{\bar{\sigma}}}{2\mu}\ln\left(1 + \frac{2\mu}{\sqrt{\bar{\sigma}}}\sqrt{-I_2'}\right)\right] \tag{A.1}$$

Where: $\bar{\sigma}$ = maximal second stress invariant

μ = shear modulus (initial tangent)

I_2' = second invariant of the deviatoric strain

Using a stress definition from Reference 14

$$\underset{\sim}{\sigma} = \frac{\partial\phi}{\partial I_1}\underset{\sim}{E} + \frac{\partial\phi}{\partial I_2}\left(I_1\underset{\sim}{E} - \underset{\sim}{\varepsilon}\right) + \frac{\partial\phi}{\partial I_3}\,\text{cofactor}\ \underset{\sim}{\varepsilon} \tag{A.2}$$

Where: ϕ = the total inner energy

$\underset{\sim}{\sigma}$ and $\underset{\sim}{\varepsilon}$ = the stress and strain tensors

$\underset{\sim}{E}$ = the unit matrix

I_1, I_2, I_3 = invariants of the strain tensor

From the fact that

$$I_2' = \frac{1}{3}I_1^2 - I_2 \tag{A.3}$$

Equation A.1 shows that ϕ_2 contributes to $\underset{\sim}{\sigma}$ through the first two terms on the right-hand side of Equation A.2. That is,

$$\underset{\sim}{\sigma}_2 = \frac{\partial\phi_2}{\partial I_2}I_1\underset{\sim}{E} - \frac{\partial\phi_2}{\partial I_2}\underset{\sim}{\varepsilon} + \frac{\partial\phi_2}{\partial I_1}\underset{\sim}{E} \tag{A.4}$$

which may be written as

$$\underset{\sim}{\sigma}_2 = -\frac{\partial\phi_2}{\partial I_2}\underset{\sim}{\varepsilon}' + \frac{\partial\phi_2}{\partial I_1}\underset{\sim}{E} + \frac{2}{3}I_1\frac{\partial\phi_2}{\partial I_2}\underset{\sim}{E} \tag{A.5}$$

where $\underset{\sim}{\varepsilon}'$ is the deviatoric strain tensor. The deviatoric stress tensor for $\underset{\sim}{\sigma}$ is

$$\underset{\sim}{S} \equiv \underset{\sim}{\sigma} - P\underset{\sim}{E} \tag{A.6}$$

Where:

$$P = \frac{\sigma_{11} + \sigma_{22} + \sigma_{33}}{3}$$

From Equation A.5, we see that for $\underset{\sim}{\sigma}_2$

$$P = \frac{\partial \phi_2}{\partial I_1} + \frac{2I_1}{3}\frac{\partial \phi_2}{\partial I_2}$$

Thus

$$\underset{\sim}{S}_2 = \underset{\sim}{\sigma}_2 - \frac{\partial \phi_2}{\partial I_1}\underset{\sim}{E} - \frac{2I_1}{3}\frac{\partial \phi_2}{\partial I_2}\underset{\sim}{E} \tag{A.7}$$

Substituting Equation A.5 into Equation A.7

$$\underset{\sim}{S}_2 = -\frac{\partial \phi_2}{\partial I_2}\underset{\sim}{\varepsilon}' \tag{A.8}$$

Thus, from Equation A.8

$$S_2 = -\left(\frac{\partial \phi_2}{\partial I_2}\right)^2 I_2' \tag{A.9}$$

where S_2 is the second invariant of the deviator stress. From Equation A.3

$$\frac{\partial \phi_2}{\partial I_2} = \frac{\partial \phi_2}{\partial I_2'}\frac{\partial I_2'}{\partial I_2} = -\frac{\partial \phi_2}{\partial I_2'}$$

From Equation A.1

$$\frac{\partial \phi_2}{\partial I_2} = \frac{\sqrt{\bar{\sigma}}}{\sqrt{-I_2'}} \left(1 - \frac{1}{1 + \frac{2\mu}{\sqrt{\bar{\sigma}}} \sqrt{-I_1'}} \right)$$

$$\frac{\partial \phi_2}{\partial I_2'} = \frac{2\mu}{1 + \frac{2\mu}{\sqrt{\bar{\sigma}}} \sqrt{-I_2'}} \qquad \text{(A.10)}$$

Using Equation A.10 in Equation A.9

$$S_2 = - \left(\frac{2\mu}{1 + \frac{2\mu}{\sqrt{\bar{\sigma}}} \sqrt{-I_2'}} \right)^2 I_2' \qquad \text{(A.11)}$$

The square root of the stress deviator is limited as indicated in Figure A.1. Thus, the current value of the shear modulus of G in the constitutive matrix $[D]$ (Equation 3.9) is defined by

$$G = \frac{2\mu}{1 + \frac{2\mu}{\sqrt{\bar{\sigma}}} \sqrt{-I_2'}}$$

However, this expression for G is programmed as a function of the first stress invariant in the form

$$G = \frac{2\mu}{1 + \frac{2\mu \sqrt{-I_2'}}{\sqrt{\bar{\sigma} + \alpha P}}}$$

where α is associated with the slope of the Drucker-Prager yield surface for the particular soil involved, and P is the first stress invariant. As can be seen in Figure A.1, this causes the stress deviator limit to depend on the first invariant of the stress tensor.

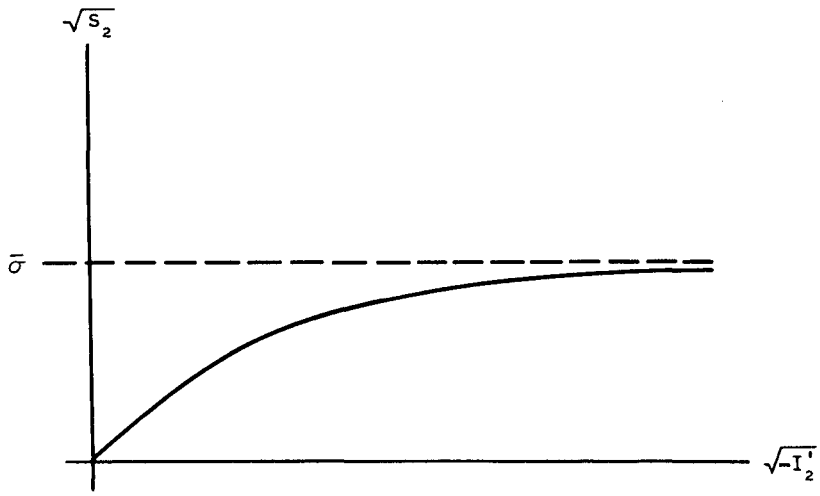

Figure A.1 Deviator stress limit.

REFERENCES

1. A. J. Hendron and others; "Design of Cylindrical Reinforced Concrete Tunnel Liners to Resist Air Overpressure"; Contract Report 68.010, June 1968; U. S. Naval Civil Engineering Laboratory, Port Hueneme, California; Unclassified.

2. W. J. Boegly, W. L. Griffin, and K. P. Nelson; "Conceptual Design of a Dual-Use Utility Tunnel Blast Shelter for White Plains, New York"; March 1969; Oak Ridge National Laboratory, Oak Ridge, Tennessee; Unclassified.

3. G. N. Savin; "Stress Concentration Around Holes"; 1961; Pergamon Press, New York, N. Y.; Unclassified.

4. J. G. Trulio; "Theory and Structure of the AFTON Codes"; Technical Report No. AFWL-TR-66-19, June 1966; Air Force Weapons Laboratory, Kirtland Air Force Base, New Mexico; Unclassified.

5. F. B. Hilderbrand; "Methods of Applied Mathematics"; Second Edition, 1965; Prentice-Hall, Inc., Englewood Cliffs, New Jersey; Unclassified.

6. W. Juanzemis; "Continuum Mechanics"; 1967; Macmillan Company, New York, N. Y.; Unclassified.

7. R. W. Clough and Y. Rashid; "Finite Element Analysis of Axi-Symmetric Solids"; Journal, Engineering Mechanics Division, February 1965, Vol. 91, No. EM1, Pages 71-85; American Society of Civil Engineers, New York, N. Y.; Unclassified.

8. P. V. Marcal and I. P. King; "Elastic-Plastic Analysis of Two-Dimensional Stress Systems by the Finite Element Method"; International Journal of Mechanical Sciences, Vol. 9, No. 3, March 1967, Pages 143-155; Unclassified.

9. E. L. Wilson; "A Computer Program for the Dynamic Stress Analysis of Underground Structures"; Report No. 68-1, 1968; University of California, Department of Civil Engineering, Structural Engineering Laboratory, Berkeley, California; Unclassified.

10. E. L. Wilson; "Elastic Dynamic Response of Axisymmetric Structures"; Report No. 69-2, January 1969; University of California, Department of Civil Engineering, Structural Engineering Laboratory, Berkeley, California; Unclassified.

11. O. C. Zienkiewicz; "Finite Element Method in Structural and Continuum Mechanics"; 1967, Pages 192-211; McGraw-Hill Book Company, New York, N. Y.; Unclassified.

12. J. G. Jackson, Jr.; "Factors that Influence the Development of Soil Constitutive Relations"; Miscellaneous Paper No. 4-908, July 1968; U. S. Army Engineer Waterways Experiment Station, CE, Vicksburg, Mississippi; Unclassified.

13. A. C. Eringen; "Nonlinear Theory of Continuous Media"; 1962; McGraw-Hill Book Company, New York, N. Y.; Unclassified.

14. F. G. Murnaghan; "Finite Deformation of an Elastic Solid"; 1951; John Wiley and Sons, Inc., New York, N. Y.; Unclassified.

15. D. Brown and R. Froelich; "Ideas from Continuum Mechanics Pertinent to the Development of Computer Codes"; Unpublished report, 1968; U. S. Army Engineer Waterways Experiment Station, CE, Vicksburg, Mississippi; Unclassified.

16. K. Höeg; "Pressure Distribution of Underground Structural Cylinders"; Technical Report No. AFWL-TR-65-98, April 1966; Air Force Weapons Laboratory, Kirtland Air Force Base, New Mexico; Unclassified.

Address	No. of Copies
Army	
Chief of Engineers, Department of the Army, Washington, D. C. 20314	
ATTN: DAEN-MER-D	1
DAEN-MEZ-A	1
DAEN-CWE	1
DAEN-CWZ-R	1
DAEN-MCE	1
DAEN-MCZ-S	1
DAEN-MCE-D	1
DAEN-ASI	2
DAEN-ZN	1
Chief of Research and Development, Department of the Army, Washington, D. C. 20310 ATTN: Director of Army Technical Information	3 copies of Form 1473
Chief of Research and Development, Department of the Army, Washington, D. C. 20310	
ATTN: CRDNCB	1
DARD-ARE	1
U. S. Army Engineer Div., Missouri River (including Omaha District), P. O. Box 103, Downtown Station, Omaha, Neb. 68101 ATTN: Office of Admin Services (Library)	3
Commandant, U. S. Army Air Defense School, Fort Bliss, Tex. 79906	1
Commandant, U. S. Army Command & General Staff College, Fort Leavenworth, Kans. 66027 ATTN: Archives	1
Commandant, Army War College, Carlisle Barracks, Pa. 17013 ATTN: Library	1
Commanding General, Aberdeen Proving Ground, Aberdeen, Md. 21005 ATTN: Director, Ballistic Research Laboratories	4
Commanding General, The Engineer Center, Fort Belvoir, Va. 22060 ATTN: Assistant Commandant, Engineer School	1
Commanding General, U. S. A. Electronics Command, Fort Monmouth, N. J. 07703 ATTN: AMSEL-GG-DD	1
Commanding General, USA Missile Command, Huntsville, Ala. 35809	1
Commanding General, USA Munition Command, Dover, N. J. 07801	1
Commanding General, U. S. Continental Army Command, Fort Monroe, Va. 23351	1

Address	No. of Copies
Army (Continued)	
Commanding General, U. S. Army Materiel Command, Washington, D. C. 20310 ATTN: AMCRD-DE-N	2
Commanding Officer, Picatinny Arsenal, Dover, N. J. 07801 ATTN: ORDBB-TK	1
Commanding Officer, Eustis Directorate, U. S. Army Air Mobility Research and Development Laboratory, Fort Eustis, Virginia 23604 ATTN: VDLEU-ADSP	1
Commanding Officer, U. S. Army Combat Developments Command, Nuclear Agency, Fort Bliss, Tex. 79916	1
Commanding Officer, U. S. Army Mobility Equipment Research and Development Center Fort Belvoir, Va. 22060 ATTN: Technical Documents Center, Building 315	1
Commanding Officer, U. S. Army Nuclear Defense Laboratory, Edgewood Arsenal Edgewood, Md. 21040 ATTN: Technical Library	1
Department of the Army, CE Ballistic Missile Construction Office, P. O. Box 4187 Norton AFB, Calif. 92409	1
Director of Civil Defense, Office of the Secretary of the Army, Washington, D. C. 20310 ATTN: Mr. George Sisson (RE-ED)	2
Division Engineer, U. S. Army Engineer Division, Ohio River, P. O. Box 1159 Cincinnati, Ohio 45201 ATTN: ORDED-FL	1
Technical Library USAMERDC, Bldg 314 Fort Belvoir, Va. 22060	1
Commander/Director, U. S. Army CRREL, P. O. Box 282, Hanover, N. H. 03755 ATTN: Mr. K. Boyd	1
Director, U. S. Army Construction Engineering Research Laboratory, P. O. Box 4005, Champaign, Ill. 61820 ATTN: Library	1
Director, U. S. Army Coastal Engineering Research Center, 5201 Little Falls Road, N. W., Washington, D. C. 20016 ATTN: Mr. T. Saville, Jr.	1
138th Engineer Group (Construction), Department of the Army, Fort Riley, Kans. 66442 ATTN: ALBFEN-O	1

Address	No. of Copies
Army (Continued)	
President, U. S. Army Air Defense Board, Fort Bliss, Tex. 79906	1
Superintendent, U. S. Military Academy, West Point, N. Y. 10996 ATTN: Library	2
Director, Explosive Excavation Research Office P. O. Box 808, Livermore, Calif. 94551	1
Director, Explosive Excavation Research Office P. O. Box 808, Livermore, Calif. 94551 ATTN: Technical Information Division	1
Navy	
Commander-in-Chief, Pacific, FPO, San Francisco 94129	1
Commander-in-Chief, U. S. Atlantic Fleet, U. S. Naval Base, Norfolk, Va. 23511	1
Chief of Naval Operations, Navy Department, Washington, D. C. 20350 ATTN: OP-75 OP-03EG	 2 1
Chief of Naval Research, Navy Department, Washington, D. C. 20390 ATTN: Code 418	1
Commandant of the Marine Corps, Navy Department, Washington, D. C. 20380 ATTN: Code A04E	2
Commander, Naval Facilities Engineering Command, Navy Department, Washington, D. C. 20370 ATTN: Code 04 Code 03	 1 1
Commander, Naval Ordnance Systems Command, Washington, D. C. 20360	1
Commander, Naval Ship Engineering Center, Washington, D. C. 20360 ATTN: Code 6115	1
Commanding Officer, Nuclear Weapons Training Center, Atlantic Naval Base, Norfolk, Va. 23511 ATTN: Nuclear Warfare Department	1
Commanding Officer, Nuclear Weapons Training Center, Pacific, Naval Station, North Island San Diego, Calif. 92136	2
Commanding Officer & Director, Naval Electronics Laboratory, San Diego, Calif. 92152	1
Commanding Officer & Director, Naval Ship Research and Development Center Carderock, Md. 20007	1
Commanding General, Marine Corps Development and Education Command, Quantico, Va. 22134 ATTN: Director, Development Center	2

Address	No. of Copies
Navy (Continued)	
Commanding Officer & Director, U. S. Naval Civil Engineering Laboratory Port Hueneme, Calif. 93041 ATTN: Code L31	2
Commanding Officer, U. S. Naval Civil Engineer Corps Officer School, U. S. Naval Construction Battalion Center, Port Hueneme, Calif. 93041	1
Commanding Officer, U. S. Naval Damage Control Training Center, Naval Base Philadelphia, Pa. 19112 ATTN: ABC Defense Course	1
Commanding Officer, U. S. Naval Weapons Evaluation Facility, Kirtland Air Force Base Albuquerque, N. Mex. 87117 ATTN: Code WEVS	1
Commanding Officer, U. S. Naval Weapons Laboratory, Dahlgren, Va. 22448 ATTN: MAL	1
Commander, U. S. Naval Oceanographic Office, Suitland, Md. 20023	1
Commander, U. S. Naval Ordnance Laboratory, Silver Spring, Md. 20910 ATTN: 241 243 240	 1 1 1
Commander, U. S. Naval Ordnance Test Station, China Lake, Calif. 93555	1
Director, U. S. Naval Research Laboratory, Washington, D. C. 20390	1
President, U. S. Naval War College, Newport, R. I. 02840	1
Special Projects, Navy Department, Washington, D. C. 20360 ATTN: SP-272	1
Superintendent, U. S. Naval Postgraduate School, Monterey, Calif. 93940	1
Underwater Explosions Research Division, Naval Ship Research and Development Center Norfolk Naval Shipyard, Portsmouth, Va. 23709	1
Air Force	
Air Force Flight Dynamics Laboratory, Wright-Patterson AFB, Dayton, Ohio 45433 ATTN: Mr. Frank Janik, Jr.	1
Air Force Institute of Technology, AFIT-L, Building 640, Wright-Patterson AFB, Ohio 45433	1
Commander, Air Force Logistics Command, Wright-Patterson AFB, Ohio 45433	2
Air Force Systems Command, Andrews Air Force Base, Washington, D. C. 20331 ATTN: DEE	1

Address	No. of Copies
Air Force (Continued)	
Air Force Technical Applications Center, Department of the Air Force, Washington, D. C. 20333	1
Air Force Weapons Laboratory, Kirtland AFB, N. Mex. 87117	
ATTN: Library	2
DEV/CPT J. C. Thompson	1
Mr. R. W. Henney	1
Director, Air University Library, Maxwell AFB, Ala. 36112	2
Commander, Strategic Air Command, Offutt AFB, Nebr. 68113 ATTN: OAWS	1
Commander, Tactical Air Command, Langley AFB, Va. 23365 ATTN: Document Security Branch	1
Space and Missile Systems Organization, Norton AFB, Calif. 92409 ATTN: MMHH/MAJ T. J. Aneffi	1
Headquarters, USAF, Washington, D. C. 20330 ATTN: AFRSTG	1
Director, Air Research and Development Command Headquarters, USAF Washington, D. C. 20330 ATTN: Combat Components Division	1
Director of Civil Engineering, Headquarters, USAF, Washington, D. C. 20330 ATTN: AFOCE	1
Director, U. S. Air Force Project RAND, Via: U. S. Air Force Liaison Office, The RAND Corporation, 1700 Main Street, Santa Monica, Calif. 90406	
ATTN: Library	1
Dr. Olen A. Nance	1
Other DOD Agencies	
Administrator, National Aeronautics & Space Administration, 400 Maryland Avenue, S. W. Washington, D. C. 20546	1
Assistant to the Secretary of Defense (Atomic Energy), Washington, D. C. 20301	1
Commandant, Armed Forces Staff College, Norfolk, Va. 23511 ATTN: Library	1
Commandant, National War College, Washington, D. C. 20310 ATTN: Class Rec. Library	1
Commandant, The Industrial College of the Armed Forces, Fort McNair Washington, D. C. 20310	1

Address	No. of Copies
Other DOD Agencies (Continued)	
Commander, Test Command, DNA, Kirtland AFB, N. Mex. 87115 ATTN: TCCOM, TCDT	2
Defense Documentation Center (DDC), Cameron Station, Alexandria, Va. 22314 (NO TOP SECRET TO THIS ADDRESS) ATTN: Mr. Myer Kahn	12
Director, Defense Nuclear Agency, Washington, D. C. 20305 ATTN: SPSS	5
Director of Defense Research and Engineering, Washington, D. C. 20301 ATTN: Technical Library Mr. Frank J. Thomas	 1 1
Director, Advanced Research Projects Agency, Washington, D. C. 20301 ATTN: NTDO	1
Defense Intelligence Agency, Washington, D. C. 20301 ATTN: DI-7B	1
Director, Weapons Systems Evaluation Group, Washington, D. C. 20305	1
Langley Research Center, NASA, Langley Field, Hampton, Va. 23365 ATTN: Mr. Philip Donely	1
Manager, Albuquerque Operations Office, USAEC, P. O. Box 5400, Albuquerque, N. Mex. 87115	1
Manager, Nevada Operations Office, USAEC, P. O. Box 1676, Las Vegas, Nev. 89101	1
National Aeronautics & Space Administration, Man-Spacecraft Center, Space Technology Division, Box 1537, Houston, Tex. 77001	1
National Military Command System Support Center, Pentagon BE 685, Washington, D. C. 20301 ATTN: Technical Library	1
U. S. Atomic Energy Commission, Washington, D. C. 20545 ATTN: Chief, Classified Tech Lib, Tech Information Service	1
U. S. Documents Officer, Office of the United States National Military Representative–SHAPE APO New York 09055	1
Other Agencies	
Aerospace Corporation, 1111 E. Mill Street, San Bernardino, Calif. 92408 ATTN: Dr. M. B. Watson	1
Agbabian-Jacobsen Associates, Engineering Consultants, 8939 South Sepulveda Boulevard Los Angeles, Calif. 90045	1

Address	No. of Copies
Other Agencies (Continued)	
Applied Theory, Inc., 1010 Westwood Blvd, Los Angeles, Calif. 90024 ATTN: Dr. John G. Trulio	1
AVCO Corporation, Research and Advanced Development Division, 201 Lowell Street Wilmington, Mass. 01887 ATTN: Mr. R. E. Cooper	1
Battelle Memorial Institute, 505 King Avenue, Columbus, Ohio 43201 ATTN: Dr. P. N. Lamori	1
Bell Telephone Laboratories, Inc., Whippany Road, Whippany, N. J. 07981 ATTN: Mr. R. W. Mayo	1
The Boeing Company, P. O. Box 3707, Seattle, Wash. 98124 ATTN: Technical Library	1
Corrugated Metal Pipe Institute, Crestview Plaza, Port Credit, Ontario, Canada ATTN: Mr. W. A. Porter	1
Defence Research Establishment, Suffield, Ralston, Alberta, Canada	1
General Research Corporation, P. O. Box 3587, Santa Barbara, Calif. 93105 ATTN: Mr. Benjamin Alexander	1
Denver Mining Research Center, Building 20, Denver Federal Center, Denver, Colo. 80225 ATTN: Dr. Leonard A. Obert	1
Dynamic Science Corporation, 1900 Walker Avenue, Monrovia, Calif. 91016 ATTN: Dr. J. C. Peck	1
Edgerton, Germeshausen & Grier, Inc., 95 Brookline Avenue, Boston, Mass. 02129 ATTN: D. F. Hansen	1
Engineering Physics Company, 12721 Twinbrook Parkway, Rockville, Md. 20852 ATTN: Dr. Vincent J. Cushing Mr. W. Danek	1 1
General American Transportation Corporation, General American Research Division 7449 North Natchez Avenue, Niles, Ill. 60648 ATTN: Dr. G. L. Neidhardt	1
General Electric Company, Missile and Space Vehicle Department, Valley Forge Space Technology Center, Goddard Boulevard, King of Prussia, Pa. 19406	1
General Electric Company, TEMPO, 816 State Street, Santa Barbara, Calif. 93101 ATTN: Mr. Warren Chan (DASIAC)	1
Chief, Structural and Applied Mechanics Branch, Bureau of Public Roads, Federal Highway Administration, Washington, D. C. 20591 ATTN: Mr. F. J. Tamanini	1

Address	No. of Copies
Other Agencies (Continued)	
IIT Research Institute, 10 West 35th Street, Chicago, Ill. 60616 ATTN: Dr. T. Schiffman	1
Lockheed Missile and Space Company, Lockheed Aircraft Corporation, 111 Lockheed Way Sunnyvale, Calif. 94086 ATTN: Dr. R. E. Meyerott	1
Los Alamos Scientific Laboratory, P. O. Box 1663, Los Alamos, N. Mex. 87544 ATTN: Report Librarian	1
Ministry of Defense, MEXE, Christchurch, Hampshire, England ATTN: Dr. Philip S. Bulson Mr. Bruce T. Boswell	 1 1
The Mitre Corporation, Route 62 and Middlesex Turnpike, Bedford, Mass. 01730	1
Physics International Company, 2700 Merced Street, San Leandro, Calif. 94577 ATTN: Dr. Charles Godfrey Mr. Fred M. Sauer	 1 1
Research Analysis Corporation, Document Control Supervisor, McLean, Va. 22101	1
Dr. John S. Rinehart, Senior Research Fellow (R.2), IER/ESSA, Boulder, Colo. 80302	1
Sandia Laboratories, P. O. Box 5800, Kirtland AFB, N. Mex. 87115 ATTN: Classified Document Division for Dr. M. L. Merritt	1
Southwest Research Institute, 8500 Culebra Road, San Antonio, Tex. 78228 ATTN: Dr. Robert C. DeHart	1
General Atomic, Division of General Dynamic Corp., P. O. Box 111, 10955 John Jay Hopkins Dr., San Diego, Calif. 92112 ATTN: Dr. K. D. Pyatt, Jr.	1
URS Corporation, 1811 Trousdale Drive, Burlingame, Calif. 94010 ATTN: Mr. Harold Mason	2
U. S. Department of the Interior, Geological Survey, Geologic Division, Branch of Engineering Geology, 345 Middlefield Road, Menlo Park, Calif. 94025 ATTN: Harold W. Olsen	1
Paul Weidlinger, Consulting Engineer, 110 East 59th Street, New York, N. Y. 10022 ATTN: Dr. M. L. Baron	1
Harry Diamond Laboratories, Library, Room 207, Building 92, Connecticut Avenue and Van Ness Street, N.W., Washington, D. C. 20438 ATTN: Mildred H. Weiner	1

Address	No. of Copies
Colleges and Universities	
University of Arizona, Tucson, Ariz. 85721	
ATTN: Dr. Donald A. DaDeppo, Department of Civil Engineering	1
Professor Bruce G. Johnston, Dept of Civil Engineering	1
Dr. George Howard, College of Engineering	1
University of Colorado, School of Architecture, Boulder, Colo. 80304	1
ATTN: Professor G. K. Vetter	
University of Detroit, Department of Civil Engineering, 4001 West McNichols Road Detroit, Mich. 48221	1
ATTN: Professor W. J. Baker	
University of Florida, Department of Mechanical Engineering, Gainesville, Fla. 32603	1
ATTN: Professor John A. Samuel	
Florida State University, Department of Engineering Science, Tallahassee, Fla. 32302	1
ATTN: Dr. G. L. Rogers	
University of Illinois, Urbana Campus, Department of Civil Engineering, Urbana, Ill. 61801	
ATTN: Professor N. M. Newmark	1
Professor A. H. S. Ang	1
Professor G. K. Sinnamon	1
Professor W. J. Hall	1
Professor A. J. Hendron, Jr.	1
Professor M. A. Sozen	1
Iowa State University of Science and Technology, Ames, Iowa 50010	2
ATTN: Professor Glen Murphy	
Lehigh University, Bethlehem, Pa. 18015	
ATTN: Dr. J. F. Libsch, Materials Research Center	1
Dr. D. A. Van Horn, Department of Civil Engineering	1
University of Massachusetts, Department of Civil Engineering, Amherst, Mass. 01002	1
ATTN: Dr. M. P. White	
Massachusetts Institute of Technology, Division of Sponsored Research, 77 Massachusetts Avenue, Cambridge, Mass. 02139	
ATTN: Dr. Robert J. Hansen	1
Dr. Robert V. Whitman	1
University of Michigan, Civil Engineering Department, Ann Arbor, Mich. 48104	1
ATTN: Professor Frank E. Richart, Jr., Consultant	

Address	No. of Copies
Colleges and Universities (Continued)	
University of New Mexico, Eric H. Wang Civil Engineering Research Facility, P. O. Box 188 University Station, Albuquerque, N. Mex. 87106	2
Nova Scotia Technical College, School of Graduate Studies, Halifax, Nova Scotia, Canada ATTN: Dr. G. G. Meyerhof	1
Pennsylvania State University, University Park, Pa. 16802 ATTN: Professor G. Albright, Dept of Architectural Engineering Professor Richard Kummer, 101 Eng. A	 1 1
Purdue University, School of Civil Engineering, Civil Engineering Building, Lafayette, Ind. 47907 ATTN: Professor M. B. Scott	1
Rensselaer Polytechnic Institute, Troy, N. Y. 12180 ATTN: Dr. Clayton Oliver Dohrenwend, Security Officer, Mason House	1
Rice University, Department of Civil Engineering, Houston, Tex. 77001 ATTN: Professor A. S. Veletsos	1
San Jose State College, Department of Civil Engineering, San Jose, Calif. 95114 ATTN: Dr. Franklin J. Agardy	1
University of Texas, Balcones Research Center, Austin, Tex. 78712 ATTN: Dr. J. Neils Thompson	1
Utah State University, Department of Mechanical Engineering, Logan, Utah 84321 ATTN: Professor R. K. Watkins	1
University of Washington, Seattle, Wash. 98105 ATTN: C. H. Norris, Department of Civil Engineering Dr. A. B. Arons, Department of Physics Professor William Miller, Department of Civil Engineering, 307 More Hall	 1 1 1
The George Washington University, Nuclear Defense Design Center, School of Engineering and Applied Science, Washington, D. C. 20006	1
Worcester Polytechnic Institute, Department of Civil Engineering, Worcester, Mass. 01609 ATTN: Dr. Carl Koontz	1
Northern Arizona University, Box 5753, Flagstaff, Arizona 86001 ATTN: Professor Sandor Popovics	1
Others	
Dr. Eugene Zwoyer, 335-A Jefferson, S. E., Albuquerque, New Mexico 87108	1
Dr. Harold L. Brode, R&D Associates, P. O. Box 3580, Santa Monica, Calif. 90403	1
Dr. Wilhelm Sommer, IM BWB, 54 Koblenz, Am Rhein 2-6, Germany	1

Unclassified
Security Classification

DOCUMENT CONTROL DATA - R & D

(Security classification of title, body of abstract and indexing annotation must be entered when the overall report is classified)

1. ORIGINATING ACTIVITY *(Corporate author)* U. S. Army Engineer Waterways Experiment Station Vicksburg, Mississippi	2a. REPORT SECURITY CLASSIFICATION Unclassified 2b. GROUP

3. REPORT TITLE

FUNDAMENTAL STUDIES OF MEDIUM-STRUCTURE INTERACTION; Report 1, FINITE ELEMENT ANALYSIS OF BURIED CYLINDERS

4. DESCRIPTIVE NOTES *(Type of report and inclusive dates)*

Report 1 of a series

5. AUTHOR(S) *(First name, middle initial, last name)*

Jesse L. Kirkland
Robert E. Walker

6. REPORT DATE	7a. TOTAL NO. OF PAGES	7b. NO. OF REFS
June 1972	71	16

8a. CONTRACT OR GRANT NO.	9a. ORIGINATOR'S REPORT NUMBER(S) Technical Report N-72-7 , Report 1
b. PROJECT NO.	
c.	9b. OTHER REPORT NO(S) *(Any other numbers that may be assigned this report)*
d.	

10. DISTRIBUTION STATEMENT

Approved for public release; distribution unlimited.

11. SUPPLEMENTARY NOTES	12. SPONSORING MILITARY ACTIVITY
	Defense Nuclear Agency Washington, D. C.

13. ABSTRACT

A finite element computer program developed by the University of California, Berkeley, was adopted and modified to perform static analysis of buried structures. Two separate variable-moduli soil models were used in the code to analyze the response of 6-inch-diameter cylinders having wall thicknesses of 1/8, 1/4, and 3/8 inch when buried to a depth of 9 inches in dry sand and subjected to a static overpressure. The computed results were compared with experimental results obtained from static tests of these cylinders in the Waterways Experiment Station Small Blast Load Generator. The computer code developed generally yielded a fair approximation of the structural response of the cylinders tested with either of the two soil models employed. The major area of discrepancy between experimental and calculated results was in the values of moment and thrust for the thicker cylinders. The nature of these discrepancies indicates that the expected lateral support of the cylinders did not develop in the experiments. This fact is explained by the possible existence of an area of low-density soil below the spring line and adjacent to the cylinder (the region where sand placement is most difficult). The code, in general, represents a reasonable method for predicting the response of buried cylinders, and undoubtedly other geometries as well. However, analysis of stiff cylinders is confounded by the fact that a detailed knowledge of the interface zone is needed because of the small motion of the spring line of such stiff cylinders.

DD FORM 1 NOV 68 1473 REPLACES DD FORM 1473, 1 JAN 64, WHICH IS OBSOLETE FOR ARMY USE.

Unclassified
Security Classification

14. KEY WORDS	LINK A		LINK B		LINK C	
	ROLE	WT	ROLE	WT	ROLE	WT
Buried cylinders						
Finite element method						
Soil-structure interaction						
Static loads						